U-series constraints on intraplate magmatism

Bernard Bourdon[1] and Ken Sims[2]

[1] *Laboratoire de Géochimie et Cosmochimie, IPGP-CNRS UMR7579, 4, Place Jussieu, 75252 Paris cedex 05 France*

[2] *Department of Geology and Geophysics , Woods Hole Oceanographic Institution, Woods Hole, MA 02543, USA*

I. Introduction

Intraplate magmatism represents approximately one tenth of the flux of magma to the Earth's surface (Sleep 1990). This type of magmatism has received much attention from petrologists and geochemists as it generally exhibits a wide range of chemical compositions compared with the more uniform mid-ocean ridge basalts. Hence, it is rather paradoxical that our understanding of intraplate magmatism is rather poor. In this chapter, we shall attempt to review what insights have been gained from using U-series to constrain the sources and processes related to intraplate volcanism.

An important feature of hotspot magmatism is that in many cases, the timing of hotspot activity seems to be decoupled from the motion of the lithospheric plate. This observation, which has been the basis for proposing the existence of mantle plumes, suggests that magmas erupted at hotspots should reveal something about the nature of the deeper mantle. Understanding the processes of hotspot magmatism should also tell us about the nature of convective motion that are responsible for hotspots. A major question about hotspots is the depth from which they originate. If they originate from the seismic discontinuity at 670 km, then, their composition tells us little about the lower mantle and the exchange between the lower and upper mantle must be restricted to a diffuse return flux. If, on the other hand, they originate from the core-mantle boundary, then they should provide some information about the D" and the global convective motion of the mantle. In the recent years, hybrid models with moving boudaries have been proposed and the boundary layer generating mantle plumes are not necessarily restricted to the cases mentioned above. There is considerable stake in better understanding the origin and nature of hotspot material.

In this contribution, we shall not specifically challenge the link between mantle plumes and hotspots that has been a paradigm in the Earth Sciences (Wilson 1963;

Morgan,1971). We shall see however that several observations that are made with U-series in fact support this theory.

In the following section, we first review some of the outstanding issues that need to be resolved to better understand intraplate magmatism. We then discuss some of the specific advances that were possible using U-series. Specific features related to magma differentiation are dealt with in the chapter by Condomines et al. (this volume).

II. Difficulties in constraining hotspot melting processes :

II.a Source composition and source heterogeneities

It has long been known that the source of hotspots is different from the source of mid-ocean ridge magmatism (Gast 1968) both on the basis of trace element systematics (e.g; rare earth elements) and long-lived isotope systems (Rb-Sr, Sm-Nd, U-Pb). Both types of tracers indicate an enrichment of hotspot material relative to the depleted mantle sampled at mid-ocean ridges. What is less clear is whether this source material is also distinct in terms of its major elements (Langmuir and Hanson 1980). There are two main reasons why this debate is still ongoing: firstly, as hotspot magmas often represent smaller extents of melting (Gast, 1968 , the experimental constraints on the composition of these lavas are difficult to obtain because it has been more difficult to perform experiments with low extents of melting until recently (Baker et al., 1995). Secondly, the amount of volatiles (CO_2 and H_2O) is generally greater in hotspot lavas than in mid-ocean ridge basalts (MORB). These volatiles will significantly depress the solidus temperature at a given pressure (Olfasson and Eggler 1983; Falloon and Green 1989, see Figure 1). The melt productivities will also be affected and the composition of melts will be greatly different. As shown by the early work of Kushiro (1968), a greater pressure in CO_2 will result in more undersaturated compositions while water will have the opposite effect. Recovering the initial source composition is difficult, such that a

full parameterization of all these effects is not a trivial task and often results in non-unique solutions.

It has also been recognized that some minor phases, such as hydrous phases (amphibole, phlogopite), or accessory phases (rutile, apatite, etc.) are sometimes present in the source of hotspots (Class et al. 1997, 1998 ; Späth et al. 1996; Hoernle et al. 1993). These phases have a strong potential for fractionating the trace elements that can be used to trace both the nature of the source material and the melting process (LaTourrette et al. 1995; Sigmarsson et al. 1998). For trace element geochemists, this has been a major challenge to identify the presence of these phases and in some cases, invert the data to calculate the bulk partition coefficients and degree of melting (Minster et al. 1978; Sims et al. 1995). The presence of hydrous phases makes it more difficult to parameterize melting reactions and predict melt compositions for a given pressure and temperature because there are fewer experimental constraints (Wendlandt and Eggler, 1980; Olfasson and Eggler 1983).

An added complexity stems from the generally large compositional range found in a single locality (e.g. Dupré et al. 1982). This is often interpreted as reflecting heterogeneities within the source of the hotspot (e.g.Lassiter and Hauri 1998). Up to five distinct components have been identified on a global basis (Zindler and Hart 1986). Some of the components can be clearly fingerprinted such as the N-MORB mantle source or the lithospheric mantle. It is far more difficult to establish what the composition of recycled components should look like (White and Hoffmann 1982; Staudigel et al. 1995; Hart 1989). One of the debates has been to decide whether a pyroxenitic component is present in the source of ocean island lavas in addition to a peridotitic component (Allègre and Turcotte 1985; Hirschmann et al. 1995; Sigmarsson et al. 1998). Melting of a pyroxenite should yield compositions and melting temperature (Figure 1) that are markedly different from a peridotite. Unfortunately, there are very few constraints on the major element composition of pyroxenite melts. Furthermore, the

modal abundances of minerals in pyroxenite differs greatly from peridotite which should also affect the relative elemental fractionation during melting.

II.b Role of the lithosphere

In most cases, the lithosphere acts as an upper boundary in the melting regime of hotspots except when they are located on the axis of a spreading center (Iceland, Galapagos). Thus, this cold lithospheric cap adds yet another complexity in understanding hotspot magmatism. Firstly, the depth of the base of the lithosphere is not always well known which means that the final pressure of melting is not always well constrained. Secondly, the lithosphere will act a cold boundary that will pertub the temperature field created by upwelling of hot material (Watson and MacKenzie 1991). It is considered that the lithosphere will only be able melt once the lithosphere has been heated by the impinging plume (Chase and Liu, 1991; Ribe 1988). This process should take a few 10-20 Ma considering the rate of heat diffusion in solids and the temperature-dependence of viscosity (Olson et al. 1988). Even if the lithosphere does not melt extensively, the interaction of plume melts with the lithosphere can potentially affect the trace element and isotope signatures of hotspot magmas (Chase and Liu 1991; Class et al. 1997, 1998).

While we do have constraints on the composition of the lithosphere from peridotite nodules carried by hotspot magmas, the information they carry is not always relevant to understanding the origin and composition of hotspot magmas. For example, the pressure determined on the basis of fluid and melt inclusions can indicate an intermediate pressure of 10 kbar (Schiano et al. 1998). This would indicate that the nodule come from the middle of the lithosphere and not from its base where magmas are likely to interact. As the lithosphere has been stable over a timescale of up to several Ga, it may have had a complex history of depletion followed by metasomatism (Pearson et al. 1995; Hawkesworth et al. 1989). The

addition of minute amounts of metasomatic melt can wildly fractionate trace elements (Galer and O'Nions 1986; MacKenzie 1989) and ultimately result in long-lived isotope signatures (Sr, Nd and Pb) that are significantly different from the asthenospheric mantle (Hawkesworth et al. 1990).

II.c Complexities in the melting region

The presence of a lithosphere with a thickness up to 100 km above the plume head obscures the observations that could be made in terms of heat flow, gravity field or seismic structure. Establishing the temperature and flow fields beneath a hotspot thus becomes a difficult exercise. Several key parameters (Fig. 2) are poorly defined and mostly results from theoretical fluid dynamics model which underlines their large uncertainty. The temperature beneath hotspot region is generally estimated to be approximately 200±100°C with large uncertainties (Shilling 1991; Sleep 1990). The temperature anomalies will induce smaller densities in the plume and the flux of the density anomalies is called buoyancy flux as defined in (Sleep 1990):

$$B = \Delta\rho Q = \rho.\alpha.\Delta T.Q \qquad (1)$$

where Q is the volume flux, ρ the density, T the temperature and α the coefficient of thermal expansion. Since the contribution of Sleep (1990) about buoyancy fluxes determined based on a fixed point approach, there has been several refinements for modelling more the buoyancy fluxes beneath hotspots (Ribe, 1996). It has been argued for example that a good estimate of buoyancy flux should take into account the excess buoyancy gained from melt depletion (Ribe and Christensen 1999). It is nevertheless widely acknowledged that there are large uncertainties on the fluxes which ultimately relate to the size of the melting region (Ribe 1996).

The mantle viscosity which controls much of the dynamics of mantle plume is not a well known parameter (Watson and Mackenzie 1991; Hauri et al. 1994). There are also additional effects such as when the mantle contains even small amounts of volatiles, as these volatiles will significantly lower the viscosity of the mantle (Hirth and Kolhstedt 1996). Once the volatiles are extracted, the increased viscosity will slow down the upwelling mantle (Ito et al. 1999).

At mid-ocean ridges, mass conservation dictates that there should be some scaling between the surface plate velocities and the vertical motions if one assumes a simple corner flow. In the case of hotspots, there is no direct geophysical observation that can be used to quantify the upwelling velocity of the plume (although buoyancy flux can provide a qualitative scale). It could be argued however, that the fixity of hotspots relative to the plate motion suggests that the upwelling velocity of hotspot has to be significantly greater than the plate velocities (Rabinowicz et al. 1990). It has also been suggested that plume heads can be deflected by the plate motion which would suggest that their upwelling velocity is affected by the slow plate motion (Griffiths and Campbell 1991). Thus, there are considerable uncertainties on the absolute upwelling velocities beneath hotspots or active intraplate magmatism.

The location of islands in the hotspot region which must related to the shape of the melting region appears to be very complex. Hotspot tracks do not define a single line of islands. There is usually more than one active volcano at a time (Hawaii), there can be two lines of volcanoes rather than one (Hawaii), or the islands can be arranged in a horse-shoe shape (Marquesas, Cape Verde, Galapagos). These latter observations have been explained by several theories : (1) the plume head could spread as a gravity current that cools and slows down as its own viscosity increases (Bercovici and Lin 1996), (2) ambient mantle can be

entrained and give rise to a ring or horseshoe shape (Griffiths and Campbell 1991), or (3) the head of the plume can shape as a torus (Griffiths 1986).

The melt migration pattern beneath a hotspot is also expected to be very different from what is observed beneath ridges or subuction zones where focusing of the melt leads to a narrow region of magmatism. Here, there is no lateral pressure gradient in the matrix that can force melt to move faster than the matrix horizontally (Ribe and Smooke 1987). Thus, melt is expected to move almost vertically which (1) should prevent thorough mixing of melts and (2) should result in a relatively wide zone of magmatism.

III. U-series as a tool for deciphering hotspot magmatism

III.a Identifying residual mineral phases

The U-series decay chain have the important property of setting itself to a state of equilibrium if it is not disturbed over approximately 1 Ma. This equilibrium implies that all the nuclides have similar activities (see Introduction, this volume). If the mantle has remained in a solid-state, there is no reason for the U-series chain to be perturbed prior to melting. Upon melting, it is expected that there will be some fractionation between the nuclides that have distinct properties, namely U, Th, Ra and Pa. Any fractionation that can be measured in intraplate lavas must therefore be recent. As fractional crystallization is not expected to fractionate the U-series nuclides from one another, the measured disequilibria is generally attributed to melting. This is a key feature of U-series nuclides compared with other trace element. By comparison, when rare earth element are used to study melting processes, one has to make assumptions about the source composition.

There are now several experimental measurements of D_U and D_{Th} values for the relevant mantle phases (Blundy and Wood, this volume): garnet, clinopyroxene,

orthopyroxene, and olivine. While Ra and Pa are thought to be highly incompatible during mantle melting, their absolute D values have never been measured and are only inferred. Based on the fact that Ra and Ba have similar ionic radii (1.40 Å and 1.35 Å) and charge (+2 for both), it is generally assumed that $D_{Ra} \approx D_{Ba}$, which has been measured. However, recent theoretical work (Wood and Blundy 1994) and measurements of Ra and Ba in glass and plagioclase separates from both Hawaiian lavas and MORB (Cooper et al. 2000; Cooper et al. submitted) indicates that most likely $D_{Ra} < D_{Ba}$. For Pa, no experimental measurements have been made and no analogs have been found, therefore it has been generally assumed that the bulk partitioning behavior of Pa is similar to that of U^{5+} (Lundstrom et al. 1994). Another constraint for D_{Pa} comes from measurements of clinopyroxene and coexisting glass, which indicate that D_U / D_{Pa} for clinopyroxene is greater than two (Pickett and Murrell 1997). In this discussion, we will assume that Ra is incompatible and behaves like Ba (an alkali-earth like Ra with a smaller ionic radius) and that Pa is a highly incompatible element whose absolute D is very small.

The length of time that the parent element spends in the melt column is critical in the ingrowth models, therefore, these models are most sensitive to the D values chosen for the parent elements U and Th. Similarly, in the case of simple batch melting, it can be shown that the ^{235}U-^{231}Pa fractionation will only depend on the partition coefficients for U :

$$\left(\frac{^{231}Pa}{^{235}U}\right) = \frac{D_U + F(1 - D_U)}{F} \qquad (2)$$

In order to use U-series disequilibria for deriving useful information about melting conditions, it is important to assess the expected fractionation from various melting conditions and mantle sources. The diagram on Fig. 3 illustrates some of the potential fractionation in for $^{230}Th/^{238}U$, $^{231}Pa/^{235}U$ and $^{226}Ra/^{230}Th$ activity ratios which are discussed below in detail. Most melting regimes will yield excesses of ^{230}Th, ^{231}Pa and ^{226}Ra.

III.a.1 Melting of a mixed peridotite-pyroxenite source.

Observations that ($^{230}Th/^{238}U$) >1 indicates that garnet is required as a residual phase in the mantle source for intraplate lavas (Cohen et al. 1994; Hémond et al. 1994; Sims et al. 1995). Although a pyroxenitic component has often been suggested as a potential source of chemically and isotopically enriched signatures in oceanic basalts (Zindler et al. 1984; Allègre, and Turcotte 1986; Hirschmann and Stolper 1996, Lassiter and Hauri, 1999), its role in causing these variations remains controversial.

If pyroxenites are present in the source of ocean island lavas, then the fractionation in ^{230}Th-^{238}U and ^{231}Pa-^{235}U is predictably distinct (Hirschmann and Stolper 1996; Stracke et al. 2000) from what would be seen in peridotites. Using the partition coefficients for garnet-pyroxenite (Hauri et al. 1994; La Tourrette et al. 1993) and garnet-peridotite (Salters and Longhi 1999) allows one to compare trace element fractionations during melting of these source components (Stracke et al. 2000). In order to take into account the source variation, a commonly used parameter is the δ(Lu/Hf) which is defined with the following equation:

$$\delta(Lu/Hf) = ((Lu/Hf)_{2Gyr} - (Lu/Hf)_m/(Lu/Hf)_{2Gyr}) \qquad (3)$$

This parameter is a direct measure of the Lu/Hf fractionation which is greater for garnet-bearing lithology such as pyroxenite. Melting of garnet-peridotite results in melts having smaller Lu/Hf fractionation {defined by δ(Lu/Hf)} and significantly larger ^{230}Th excesses compared to melts from a garnet-pyroxenite with similar degrees of melting (Figure 3b-c and Figure 4). Sm/Nd fractionation (defined by δ(Sm/Nd) shows large variations with the degree of melting, but the variation is larger in garnet-peridotite melts than in garnet-pyroxenite melts. In the case of melting of a pyroxenite-peridotite mixture, it is expected that the pyroxenite will melt to a large degree while the peridotite will melt to a smaller extent.

For increasing extents of melting, the melt will become richer in a peridotite component which is characterized by larger $^{230}Th/^{238}U$ and smaller δ(Lu/Hf). As shown on Fig. 4, the Hawaian data trend is exactly the reverse of the predicted trend for a mixed pyroxenite-peridotite lithology.

In addition, garnet-peridotite melts are expected to have a more depleted isotopic signature than garnet-pyroxenite melts (see e.g Allègre and Turcotte, 1986; Hirschmann et al. 1995; Lundstrom et al. 1998 ; Sigmarsson et al. 1998) . Thus, garnet-pyroxenite melts are clearly distinguishable from garnet-peridotite melts in terms of combined δ(Lu/Hf), δ(Sm/Nd), ($^{230}Th/^{238}U$), $^{176}Hf/^{177}Hf$, and $^{143}Nd/^{144}Nd$. Based on all these arguments and measurements of U-Th disequilibria and Nd and Hf isotope for young Hawaiian basalts, Stracke et al. (2000) suggested that the combined Hf-Nd-Th isotope and trace element data can distinguish between melts derived from peridotitic and pyroxenitic sources, and exclude the existence of garnet-pyroxenite in the source of Hawaiian basalts (Stracke et al. 2000).

Another argument against a pyroxenite component comes for U and Th measurements in pyroxenites and associated peridotites plotted as a histogram (Figure 5). These data show that pyroxenites do not have a greater Th/U than peridotite as had been argued by Sigmarsson et al. (1998) for the case of the Canaries and Hawaii. While $^{230}Th/^{238}U$ and Th/U data form an inclined array that could represent a mixing line, the endmembers are unlikely to be pyroxenite and peridotite. If one is to interpret these arrays with mixing, they could represent mixtures between depleted and enriched peridotites.

III.a.2 Melting of the lithospheric mantle

There are several signatures that can be used to trace lithospheric melting with U-series disequilibria. First, lithospheric melting should be shallower and therefore have a

weaker garnet signature than asthenospheric melting. Second, the lithosphere can be hydrated and contain phases that are only stable at intermediate pressure such as amphibole. Third, the lithosphere can be characterized by a distinct Th/U ratio that can be traced using $^{230}Th/^{232}Th$ activity ratios. This last point will be discussed in section IIIc.

At shallow pressure (less than 1 GPa), Th becomes slightly more compatible than U in clinopyroxene (Landwehr et al. 2001) and garnet is not stable even in pyroxenite or eclogite. On the other hand, it is believed (mostly based on observations) that Pa remains more incompatible than U through the entire length of the melt column. Thus, melting at intermediate pressure should yield small ^{230}Th or ^{238}U excesses and ^{231}Pa excess. This is indeed what has been observed in the lithospheric mantle in the Colorado plateau by Asmerom et al. (2000). The depth of melting in this region is approximately 2 GPa while the prediction for equal D_{Th} and D_U is 0.8-1.3 GPa (Landwehr et al. 2001). This apparent discrepancy might reflect what Asmerom et al. (2000) suggested which is a reequilibration of the melts produced at the base of the lithosphere at shallower pressure. If there is such a reequilibration, then the initial excess ^{230}Th would decrease while the ^{231}Pa excess could be maintained as advocated for the Comores (Bourdon et al., 1998) or the East Pacific Rise (Sims et al., in press).

Another index of a shallow production or equilibration of melt are the ^{226}Ra deficit found in some ocean island basalts. Several hydrous minerals such as amphibole and phlogopite are thought to incorporate more Ba than Th. As Ba is used is an analogue for Ra , it can be inferred that the amphibole partition coefficient for Ra will also be greater than for Th. Using the approach of Blundy and Wood (1994), the partition coefficient of Ra in amphibole can be estimated to be 0.03 which is much greater than the value for Th in this same mineral (LaTourrette et al. 1995). Thus, it can be predicted that melting of an amphibole or phlogopite-bearing peridotite should yield ^{226}Ra deficits (Claude-Ivanaj et al.

1998, 2001) if the mode of amphibole is greater than a few percent. Such deficits were first reported in the Azores by Widom et al.() for a differentiated trachyte and interpreted as due to alteration. Claude-Ivanaj et al. (1998) also found lavas from the La Grille volcano, Comores that had an amphibole signature on the basis of trace elements and a smaller ^{226}Ra excess than the nearby Karthala lavas that has no amphibole signature.

It is worth noting that in the case of melting with an amphibole residue, most of the ^{238}U resides in garnet or clinopyroxene because $D_U^{garnet}/D_U^{amphibole}$ is close to 10. Thus, the ^{226}Ra which is produced by decay of ^{238}U must initially reside in garnet. The timescale for garnet/amphibole chemical equilibration with respect to Ra is of the order of $t \approx a^2/D_{Ra}$, where a is the mean radius of an amphibole and D_{Ra} the diffusion coefficient of Ra in silicate minerals. Upon melting, only a fraction of this radium can reequilibrate and be incorporated within the amphibole. Thus, the presence of Ra deficit or smaller Ra excess provides strong constraints on the degree of melt equilibration prior to melt extraction (Van Orman and Bourdon, in prep).

III.a.3 Melting with accessory phases

It has been advocated that in some cases, accessory phases such as apatite, monazite rutile or zircon could play a role in fractionating U-series during melting. These phases are potentially important as they have large partition coefficients for U and Th. This was discussed theoretically by Beattie (1993) who showed that based on the mantle abudances of P_2O_5 and ZrO_2, it was unlikely that there was significant amounts of apatite and zircon in the mantle. For these phases to significantly affect the relative compatibility of Th and U, their abundances has to be such that:

$$X_a \approx \frac{\sum_{i \neq a} X_i D_i}{D_a} \qquad (4)$$

Beattie (1993) showed rather convincingly that only zircon could have a significant effect but zirconium is also present in garnets and clinopyroxenes such that zircon is extremely unlikely in mantle assemblages.

There are several trace-element ratios which should be diagnostic indicators of many of these accessory phases... For example, if one assumes that rutile is a residual phase during melting of pyroxenite (Sigmarsson et al. 1998), then considering the large Nb partition coefficient in rutile, large Nb deficits are expected in the melt relative to U. In the case of Lanzarote (Sigmarsson et al. 1998), it is found that the samples with the smallest Nb/U ratios do not have the largest ($^{230}Th/^{238}U$) activity ratios (Figure 6). Similarly, the most radiogenic $^{87}Sr/^{86}Sr$ ratios which should indicate the presence of pyroxenite do not correspond to the lowest Nb/U ratios which should be found in the rutile-bearing pyroxenite. Thus, it is unlikely, that rutile is a residual phase during melting (Sims and DePaolo 1997)., While the presence of these phases could explain some of the fractionation found in OIB, its presence remains to be demonstrated.

III.b Role of source heterogeneities on melting processes.

In this section, we discuss how source heterogeneities could affect the rate of magma production per unit of time, which is an essential parameter in predicting U-series fractionation. It can be shown simply that if one considers that the rate of melt migration is fast relative to the half life of the daugher isotope, then the magnitude of the fractionation between a daughter isotope and its parent depends directly on the rate of magma production (see discussion below). It has been argued that the melting rate, (generally given in $kg.m^{-3}.a^{-1}$) could vary depending on the source composition (Hirschmann et al. 1999; Turner et al. 1997), but also on phase transitions as the mantle upwells (Asimow et al. 1995). These effects will also depend on the process of magma extraction. This can be shown simply in the case of wet

melting. If the melt is rapidly extracted from the source region and no longer interacts with the matrix, once the volatiles are completely partitioned into the melt, further melting will be equivalent to melting of a dry peridotite. It has been shown also that more fertile source have slower melting rates at least at the inception of melting (Hirschmann et al. 1999).

Although these considerations are theoretically sound, there are very few case studies where these complexiities could be demsontrably shown but it has been argued in several contributions that they could play a role (Hirschmann et al. 1999, Turner et al. 1997). It has been argued in the case of the Azores region that the volatile content in the source is larger than in N-MORB mantle. As argued by Turner et al. (1997), the lower $^{230}Th/^{238}U$ activity ratios found for the Sao Miguel lavas, Azores could be due to a faster melting rate of an enriched source.

III.c Tracing mantle sources

III.c.1 Global systematics

U-series disequilibria offers another probe for mantle processes whose application has been largely pioneered as reported in Condomines et al. (1988) and Allègre and Condomines (1982). Many applications are reported in Gill et al. (1992) and Allègre et al. (1988). If one assumes that the mantle melts according to a batch melting process, then measured $^{230}Th/^{232}Th$ ratios in lavas should reflect the Th/U ratio in the mantle source of the lavas and the Th/U ratio of the source can be calculated with the following equation:

$$\frac{^{232}\mathrm{Th}}{^{238}\mathrm{U}} = \frac{\lambda_{238}}{\lambda_{232}\left(^{230}\mathrm{Th}/^{232}\mathrm{Th}\right)} \qquad (5)$$

where λ_{232} and λ_{238} are decay constants for ^{232}Th and ^{238}U respectively and parenthesis denote activiy ratios. This provides a very important tool for understanding mantle processes. While other radiogenic isotope tracers (Sr, Nd and Pb) respond slowly to a change in

parent/daughter ratio (e.g. Rb/Sr), in the case of Th isotopes, after approximately 300 ka, the $^{230}Th/^{232}Th$ directly reflects the mantle source compositions. Thus, the global correlation found between Th/Us and $^{87}Sr/^{86}Sr$ for MORB and OIB indicate that the Th/U ratio in the mantle source is long-lived and consistent with the indication given by $^{87}Sr/^{86}Sr$ (Figure 7). This negative correlation supports the idea that the depleted mantle is complementary to the more enriched continental crust. This correlation is also consistent with the correlation between Sr and Nd isotope ratios for MORB and OIB.

This correlation has been further extended with recent measurement of basalts from Samoa, which have extremely high $^{87}Sr/^{86}Sr$ (0.708) and low $^{230}Th/^{232}Th$ (Sims and Hart in prep), which clearly shows that the functional form of this relationship is hyperbolic rather than linear as has been previously suggested (Figure 7). While this plot emphasizes the influence which source compositions can have on the $^{230}Th/^{232}Th$ of OIBs like Samoa, MORB, on the other hand, show little variability in $^{87}Sr/^{86}Sr$, but significant variability in $^{230}Th/^{232}Th$, indicating that there is a significant ingrown component of ^{230}Th resulting from slow melting (see below).

As advocated by Allègre et al. (1986), the Th-Sr can be used to determine the Th/U ratio of the bulk silicate Earth based on an estimated value of $^{87}Sr/^{86}Sr$ of 0.7045-0.705. A similar approach can be used with $^{208}Pb^*/^{206}Pb^*$ where as there $^{208}Pb^*/^{206}Pb^*$ is defined as follows:

$$\frac{^{208}Pb^*}{^{206}Pb^*} = \frac{\frac{^{208}Pb}{^{204}Pb} - \left(\frac{^{208}Pb}{^{204}Pb}\right)_{CD}}{\frac{^{206}Pb}{^{204}Pb} - \left(\frac{^{206}Pb}{^{204}Pb}\right)_{CD}} \qquad (6)$$

There is a positive trend between $^{208}Pb^*/^{206}Pb^*$ and Th/U_s which is better defined using a compilation of mass spectrometry data (Fig. 8) than in the original paper by Allègre et al . (1986). Another line that can be defined in this diagram is the $^{208}Pb^*/^{206}Pb^*$ ratio calculated

assuming that the bulk silicate Earth has evolved as a closed system since 4.55 Ga for a range of Th/U ratios. The correlation defined by OIB and MORB yields an intersect of 4.2. It was argued that this intersect defines the Th/U ratio of the silicate Earth (Allègre et al. 1986). For this argument to be complete, data for the continental crust should plot on the other side of the closed-system line on this diagram since this reservoir represents roughly 50% of the Th-U budget of the Earth.

III.c.2 Tracing recent metasomatism

The global systematics in Th isotope geochemistry are outlined above and generally show a consistency between long-lived isotope systems and Th isotopes which respond readily to mantle processes. Where there are deviations from these systematics, it is possible to put some constraints on processes that may have modified the mantle source composition prior to melting. This is particurlarly useful in tracing metasomatism. Metasomatic melts should have fractionated U from Th. It these melts get frozen in the lithospheric mantle, they will in the long-run impart a specific $^{230}Th/^{232}Th$ signature. A recent metasomatic enrichment will not necessarily modify the Sr or Pb isotope signature but the Th isotopes will be affected. Thus, a decoupling between $^{230}Th/^{232}Th$ and $^{87}Sr/^{86}Sr$ or $^{208}Pb^*/^{206}Pb^*$ should be detected. Elevated $^{230}Th/^{232}Th$ would for example correspond to an enrichment of U relative to Th. This is particularly obvious in the case of the Great Rift lavas which are well above the Th-Sr trend defined for continental and oceanic basalts (Fig. 7). It is hard to put a precise time scale on these effects because for a given end-point several paths are possible (see Fig. 8). It is possible nevertheless to give an upper limit for the timescale of enrichment. In the case of the Crater of the Moon lavas, Great Rift, for $^{238}U/^{204}Pb$ ranging between 8 and 10, it would take 100 to 200 Ma to significantly modify the $^{208}Pb^*/^{206}Pb^*$ ratios as shown on Fig. 8. This

relatively recent enrichment has been interpreted by Reid as reflecting metasomatism by U-rich fluid related to the Yellowstone mantle plume which would have lowered Th/U ratios. An alternative explanation would be that the lithosphere has been metasomatized by U-rich subduction related fluids.

In contrast with the Great Rift lavas, continental lavas from the Gaussberg volcano are characterized by high Th/U ratios (low $^{230}Th/^{232}Th$) (Williams et al. 1992). These high Th/U (up to 7.5) ratios are attributed to repeated metasomatic events in the subcontinental lithosphere (Fig. 8). Recent experiments by LaTourrette et al. (1995) have shown that the partition coefficients of U and Th in phlogopite are small (10^{-3}) and close to each other. Thus, the large Th/U found in the Gaussberg lavas can no longer be explained by the presence of phlogopite. Similarly, residual phlogopite does not preclude the large ^{230}Th excesses found in the Gaussberg lavas. It is likely that the large ^{230}Th excess (1.44-1.58) can be attributed to small degree melts with a garnet or clinopyroxene residue and does not require disequilibrium melting as advocated in Williams et al. (1992).

IV. Melting processes and relation to convective structure of plume

IV.a Time dependent melting models for hotspot magmatism

There is considerable evidence indicating that the dominant mode of melt production in intraplate volcanism is adiabatic decompression of solid upwelling mantle material in the form of mantle plumes. In this scenario, the formation and transport of basaltic magma during adiabatic decompression of mantle rock can be characterized in terms of several rate dependent parameters: the velocity of the upwelling (solid) mantle, the rate of melting, the melt velocity and the storage time of magma before eruption (e.g., Stolper et al., 1981; Turcotte, 1982; McKenzie, 1984; 1985; Richter and McKenzie, 1984; Ribe, 1985; 1987; DePaolo, 1996). While numerous physical models have now been developed which describe

the generation and transport of basaltic magma from the Earth's mantle, they suffer in application because of an incomplete knowledge of the physical properties of solid and liquid rock material, which control the time and length scales. Although it would be desirable to measure these physical parameters in order to improve this situation, and some progress is being made in this regard, the critical properties- the effective viscosities of solid and liquid rock material and the permeabilities of partially molten materials- are hard to measure or even estimate (Kohlstedt et al., 1999).

For this reason it has been desirable to pursue other approaches to constrain the timescales of magma genesis; and in this regard, U-series disequilibria has played an important role. The half-lives of ^{230}Th (75,300 yrs.) and ^{226}Ra (1,600 yrs.) of the ^{238}U decay series bracket the time scales over which melting and melt extraction are thought to occur, and large differences in the solid/liquid partitioning behavior of U, Th, Pa and Ra produce large parent-daughter fractionations during the early stages of melting. Therefore, measurement of ^{238}U -^{230}Th and ^{230}Th -^{226}Ra disequilibria in young mantle-derived basalts should, in principle, provide information on the rate of melting, the melt migration velocity and the extent of mantle melting.

Several models relating the isotopic effects of U-series disequilibria to the timescales of the melting process have now been proposed (e.g. McKenzie, 1985; Williams and Gill, 1989; Spiegelman and Elliott, 1993; Qin, 1992; Iwamori, 1994; Richardson and McKenzie, 1994). While these models differ mainly in their treatment of the melt extraction process (i.e. reactive porous flow vs near fractional melting), because they incorporate the effect of radioactive ingrowth and decay of the daughter isotopes (e.g. ^{230}Th) during melt production they are able to predict mantle melting rates and melt transport rates, based upon U-Th-Ra

and U-Pa disequilibria. These U-series mantle melting rates can, in turn, be combined with theoretical predictions of melt productivity (e.g., McKenzie and Bickle 1988; Asimov et al. 1997) to calculate a model solid mantle model upwelling rate.

U-Th-Ra and U-Pa have now been measured in several OIB suites, by high precision mass spectrometric methods (Sims et al, 1995, 1999; Cohen and O'Nions, 1993, Turner , 1997 ; Bourdon et al., 1998 ; Claude-Ivanaj 1998 ; 2001 ; Pietruszka et al.,2000 and many others). Though a number of factors such as source heterogeneity and the degree of partial melting can complicate the interpretation of the U-series data in terms of the timescales of the melting processes, the influence of mantle upwelling on the measured disequilibria is clearly distinguishable. For example, the influence of mantle upwelling is seen on the scale of individual plumes like Hawaii (Fig. 13), where the solid mantle upwelling velocity determined from U-Th and U-Pa disequilibria, decreases as a function of radial distance from the plume center (Sims et al., 1999). In the following section we, we briely review the two different end-member melting models, which incorporate the timescales of the melting process. We then show, through examples, how the the U-series data can then be compared with these models to place unique temporal constraints on many of the magmatic processes associated with intraplate volcanism.

IV.a.1 Chromatographic Porous Flow

The steady state chromatographic porous flow melting model of Spiegelman and Elliot (1993) accounts for the duration of melt generation (i.e., the time it takes the upwelling mantle to traverse the melt column), the relative velocity of the upward-percolating melt and the residual solid, and the effects of continuous melt-solid interaction during melt transport. The model assumes that chemical equilibrium is maintained between migrating liquid and the

solid matrix. This corresponds to an infinite Damköhler number, which represents the ratio of the time scale necessary for melt migration divided by the time scale for equilibration by diffusion:

$$D_a = \frac{3DL\rho_s(1-\phi)}{w_0 a \rho_m \phi} \qquad (7)$$

where L denotes the length of the melting column, a is the grain size and D the diffusion coefficient. Other parameters are given in Table 1. Continuous melt-solid interaction produces chromatography; different elements travel through the melt column at different velocities according to their relative melt/solid partition coefficients (i.e. D values). For non-radioactive elements, the steady-state chromatographic porous flow melting model produces trace-element enrichments that are identical to those of equilibrium batch melting (Spiegelman and Elliott, 1993). However, for the U-decay-series isotopes, which have half-lives that are comparable to the melt migration time scales, the chromatographic effect has a significant influence on the resulting concentrations and activity ratios. If the daughter isotope is more incompatible than the parent isotope, which is true for all of the systems considered here, the residence time of the daughter isotope in the melting column is shorter relative to the parent nuclide. This implies that the production of daughter nuclides is enhanced relative to its decay in the melting column and this produces large excesses in daughter isotopes in the resultant basaltic liquids. The extent of this daughter nuclide enhancement depends on the half life of the daughter nuclide, and consequently it is very large for Ra, and much smaller for ^{230}Th and ^{231}Pa. The extent of ingrowth, is also dependent upon the length of the melting column, with longer melt columns leading to greater enhancements of the daughter nuclides (see appendix for a more quantitative discussion of this).

The 1-D chromatographic porous flow model of Spiegelman and Elliott has seven variable parameters: the solid velocity (W), the liquid velocity (w), the porosity (ϕ), the height of the melting column (Δz), the melt fraction (F_{max}), the melting rate (Γ) and the mineral melt partition coefficients for the trace-elements being considered. The simplest way to use the U-series data and the chromatographic porous flow model to obtain estimates on time dependent parameters of melting is to use experimental constraints to estimate the height of the melt column, the melt production rate and the mineral partition coefficients and then to compare the measured U-series data with a forward model which calculates porosity and melting rate. Both numerical and analytical solutions can be used to calculate the U-series activity ratios for the 1-D chromatographic porous flow of Spiegelman and Elliott. These solutions show that that ($^{226}Ra/^{230}Th$) disequilibrium is controlled mostly by the porosity of the melt region (which controls the velocity of the melt relative to the solid) for melting rates ranging less than $2x10^{-2}$ $kg.m^{-3}.a^{-1}$. For faster melting rates, the short melting timescale does not allow enough in-growth of ^{226}Ra and becomes a limiting factor. In contrast, ($^{230}Th/^{238}U$) and ($^{231}Pa/^{235}U$) disequilibria are controlled more by the melting rate (which is related to the solid mantle upwelling rate) (Fig. 9 and 10). However, because the numerical solution takes into account a depth dependent porosity structure, whereas the analytical solutions assume a constant porosity over the length of the melting column, the absolute values of these determined parameters are significantly different depending on the initial assumptions of the porosity structure of the mantle (see appendix or Sims et al. 1999, which explicitly discusses the contrast between the analytical and numerical solution for the Spiegelman and Elliott 1993 model.) Also, as will be discussed below, the trace element partition coefficients used for the modeling can have significant influence over the resulting parameters.

Finally, with regard to the chromatographic melting model, it is also important to note that because this model takes into account the time-scale of melt migration the velocity of the melt can be determined explicitly. Since the analytical solutions assume a constant porosity the melt velocities are also constant throughout the melting column. Whereas with the numerical solution, melt velocity varies as a function of the porosity distribution of the melt column, and therefore in this case, it is more useful to calculate melt transport times by integrating the melt velocity over the length of the melt column.

IV.a.2 Dynamic Melting

In the "dynamic melting" model, as formulated by McKenzie (1985), melts produced in the upwelling mantle remain trapped, and in equilibrium with the solid residue until a critical threshold porosity is reached, after which any produced melt in excess of the threshold value escapes instantaneously. Dynamic melting takes into consideration the time-scale of the melting process and consequently, like the Spiegelman and Elliott model, produces enhanced excesses of short-lived daughter nuclides like ^{226}Ra. Dynamic melting differs from chromatographic melting in that melts move instantly to the surface as they form and do not react with the solid on the way. Because most of the uranium is extracted near the base of the melting column, disequilibria is created only at the bottom of the melt column instead of throughout . Unlike chromatographic porous flow where melt velocities are determined explicitly, with dynamic melting, melt velocities are constrained by the shortest half-life of the daughter nuclides not in radioactive equilibrium with its immediate parent (e.g., ^{226}Ra). Above the point where the threshold porosity is reached, the porosity of the melt zone is constant. Whereas the Spiegelman and Elliott model is an "infinite Damköhler number" model (melt-solid reaction is very fast relative to melt migration velocity), the dynamic melting model is a "zero-Damköhler number" model. The reality is of necessity somewhere in

between (e.g., see Hart, 1993). The dynamic melting model also differs from the Spiegelman and Elliott model in that the trace element enrichments in the melts are intermediate between batch melting and accumulated fractional melting, depending on the value of the threshold porosity relative to the distribution coefficients of the element(s) considered (Williams and Gill, 1989; Zou and Zindler, 1996). This porosity plays an important role in slowing down the extraction of the incompatible element from the solid. With a small porosity, dynamic melting is close to fractional melting where incompatible elements are efficiently stripped from the residue, while with a large porosity, it is more akin to batch melting where incompatible elements reside in the solid longer .

Dynamic melting models provide results that are similar to those obtained from the chromatographic porous flow melting model in that the extent of (^{226}Ra/^{230}Th) disequilibrium is controlled mainly by the porosity of the melt region, and (^{230}Th/^{238}U) and (^{231}Pa/^{235}U) disequilibrium mainly by the melting rate (Fig. 9 and 10) . However, with dynamic melting the time-scale of melt migration is not considered. Therefore, for a given set of partition coefficients, the dynamic melting model requires threshold or escape porosities which are lower (about a factor of 1.5) than the maximum porosity at the top of the melt zone predicted by a chromatographic melting model. With dynamic melting, the inferred melting rates are also slightly lower. This stems from the shorter residence time for the parent nuclide in the melting column obtained with dynamic melting.

IV.b Sources of Uncertainty in these models

IV.b.1 Uncertainties in sample ages and magma storage times.

Because of the relatively short half-lives of the U-series daughter isotopes, as samples age on the surface or during magma storage prior to eruption, the parent/daughter activity

ratios will decay toward their equilibrium value. If this sample age is old and unknown or if the magma storage is significant and not corrected for, one would infer too small an amount of parent/daughter fractionation for the melting process. Therefore it is important to explicitly know the samples age and to have some constraints on magma storage time when evaluating melting processes using U-series disequilibria. This issue is most significant for ^{226}Ra; and is probably not a significant source of uncertainty for the longer-lived ^{230}Th and ^{231}Pa. For example, it was shown by Vigier et al. (1999) that tholeiitic lavas from the 1978 Ardoukoba eruption in the Afars had ^{226}Ra/^{230}Th ranging from 1.93 and 1.35. Since the ^{226}Ra/^{230}Th ratios correlated with indices of magma differentiation, these results were interpreted as reflecting variable residence times in a magma chamber. Since ^{226}Ra is largely controlled by the porosity of the melt zone, uncertainties in sample ages and magma storage times translate to large uncertainties in the calculated porosity.

IV.b.2 Uncertainties in measured U, Th, Ra Partition coefficients

Calculated porosities and melting rates from both the chromatographic and dynamic melting models are highly dependent upon the absolute and relative values chosen for the U, Th, Pa and Ra partition coefficients (Table 2). The length of time that the parent element spends in the melt column is critical in the ingrowth models, therefore, these models are most sensitive to the D values chosen for the parent elements U and Th. For the combined U-Th-Ra disequilibria, the value chosen for D_{Th} is particularly important, as Th is both a parent and daughter isotope and therefore its D value affects both (^{230}Th/^{238}U) and (^{226}Ra/^{230}Th) disequilibria. For example, with the chromatographic porous flow model, in order to produce a given degree of (^{230}Th/^{238}U) and (^{226}Ra/^{230}Th) disequilibrium, decreasing the value of D_{Th} by a factor of 3 (while holding D_U and D_{Ra} constant) changes the inferred porosity by an order of magnitude for large melting rates and by up to a factor of 3 for low melting rates. In the

above modeling, it is also assumed that the U-Th-Ra partitioning is controlled by major phases (olivine, pyroxene and garnet) and that partitioning of U, Th, Pa and Ra between the melt and solid is constant throughout the melting column. While it can be reasoned that the partitioning of U, Th, (and Ra and Pa?) is controlled by the major mantle phases (Beattie, 1993a,b; La Tourrette et al., 1993) it has been recently shown that the values of mineral/melt partition coefficients can be highly dependent on the chemical compositions of the minerals as well as the temperature and pressure of the experiments. In fact, recent high-pressure experiments show that D_U and D_{Th} values can vary by as much as a factor of 10 due to variations in mineral composition and pressure (Beattie, 1993a,b; La Tourrette, 1993; Lundstrom et al, 1994; Salters and Longhi, in review, Blundy and Wood, this volume). The large variations between the different experimentally determined D_U and D_{Th} values for clinopyroxene and garnet (see Compilation of Table 2) result in large variations in the calculated porosities and melting rates for both chromatographic and dynamic melting models (Figures 9 and 10). Until these issues are resolved and the effect of chemical composition, temperature and pressure, and melt structure on the measured partitioning values for U, Th, (and Pa and Ra) are established, calculated solid mantle upwelling rates and porosities based upon ($^{230}Th/^{238}U$) ($^{226}Ra/^{230}Th$) and ($^{231}Pa/^{235}U$) disequilibria must be considered as preliminary estimates only.

IV.c Observational constraints

IV.c.1 U-series systematics for ocean island basalts

On a global basis, ocean island basalts are characterized by $^{230}Th/^{238U}$ activity ratios greater than one which suggests that they were generated by melting of garnet or high-pressure clinopyroxene. This is particularly clear when looking at the compilation shown on Fig. 11 where all the OIB plot to the left of the equiline. Chabaux and Allègre (1994) had

shown that there is a general positive correlation between $^{230}Th/^{238}U$ and $^{226}Ra/^{230}Th$ which they interpreted as due to melting. More information can be gained by considering also ^{231}Pa-^{235}U systematics (Pickett and Murrell 1997; Bourdon et al. 1998; Bourdon and Turner in prep; Sims et al. 1999). As pointed out by Pickett and Murrell (1997), the ocean island basalts define a linear trend that is clearly distinct from the MORB trend. This observation still holds based on a larger data base (Fig. 12). Bourdon et al. (1998) had shown that these two trends could be explained by variable cpx:garnet ratio in the mantle source. The variation in cpx:garnet mode could simply reflect variation in the initial pressure of melting. For deeper melting, the cpx:garnet mode should be smaller. In the context of a simple batch melting model, the recent partitioning data of Landwehr et al. (2001) as a function of pressure produces melting trends that are consistent with melting at a pressure deeper than the garnet-spinel transition (Fig. 12). As argued by Bourdon et al. (1998), the range in ($^{230}Th/^{238}U$) can be produced by variation in the upwelling rates. In contrast to OIB, MORB must have been produced by a shallower average depth of melting and are characterized by larger ^{231}Pa excess at a given $^{230}Th/^{238}U$.

IV.c.2 Constraints on mantle upwelling velocities from ^{230}Th and ^{226}Ra disequilibrium

It was shown by Chabaux and Allègre (1994) that there is a broad correlation between $^{230}Th/^{238}U$ and the buoyancy flux as estimated by Sleep (1990). The original interpretation of Chabaux and Allègre (1994) was that the range in $^{230}Th/^{238}U$ that roughly correlated with $^{226}Ra/^{230}Th$ was due to variation in the degree of melting. In fact, this correlation can also be interpreted as reflecting variation in the mantle upwelling rates. It can be shown that there is a direct link between the buoyancy flux and the upwelling velocity. In the case of a pipe flow, the buoyancy flux Q as defined by Sleep (1990) should scale with the square of the

mantle upwelling velocity W (Bourdon et al. 1998). The volumetric flux within a cylinder is equal to:

$$Q=W\pi r^2 \qquad (8)$$

The average velocity in a pipe with a circular section is given by:

$$W=\Delta\rho g r^2/8\mu \qquad (9)$$

Where μ is the viscosity. It follows that the buoyancy flux Q ($=\Delta\rho Q$) is proportional to the square of the average upwelling velocity in the pipe:

$$Q_P=(8\pi\mu/g)W^2 \qquad (10)$$

For the range of buoyancy fluxes found in mantle plumes (0.5-11 $Mg.s^{-1}$), the mantle upwelling velocities should vary by a factor of 3-4. This was shown by Bourdon et al. (1998) to be consistent with the range in ^{230}Th-^{238}U and ^{231}Pa-^{235}U disequilibrium found for ocean island basalts.

IV.c.3 Hawaiian Plume Dynamics: Evidence for a fast upwelling plume with structure :

One of the most widely studied (and perhaps the most well understood) examples of ocean island volcanism is the Hawaiian Archipelago. The islands of Hawaii are at the southeastern end of a linear chain of volcanic islands which form part of the 6000 km long Hawaiian-Emperor volcanic ridge. These islands are generally thought to be the surface expression of a stationary mantle plume that has been sitting beneath the westward moving Pacific plate for about 75 Myr. Based on the volume and composition of these basalts, as well as geophysical observations such as the geoid height and bathymetric swell, it is generally thought that the northwest motion of the Pacific plate is moving the hotspot center off the main island of Hawaii, and that the new submarine volcano of Loihi to the southeast represents the initial stages of melting produced at the leading edge of the plume.

Numerous studies on lavas from the Hawaiian Islands have shown that over the life-span of a volcano, the major- and trace-element chemistry of the erupted basalts vary significantly and systematically (MacDonald and Katsura 1964; Chen and Frey 1985). This variation is believed to be the result of movement of the Pacific plate, over the stationary mantle plume, and is typified into four distinct phases of volcano evolution: (1) a pre-shield stage,during which both tholeiitic and alkaline lavas are erupted; (2) a tholeiitic shield-building stage, which represents about 98% of the volcanoes total volume ; (3) a post-caldera or post-shield stage during which the lavas become more alkalic in composition and erupt as as small parasitic cones, forming a thin veneer over the shield stage tholeiites ; and (4) a late or rejuvenated alkalic volcanism, which occurs after an ill-defined period of quiescence. While the time required for the entire evolution of one volcano (ca 2-5 million years) is much longer than the time-span addressable by U-Th disequilibria, it is possible to obtain from several different volcanoes a suite of historic or young radiocarbon dated lavas which range in composition from primitive tholeiite to primitive alkali basalt and collectively encompass all four stages of Hawaiian volcano evolution.

Past U-series work on Hawaii, has included both early alpha counting studies (Krishnaswami, 1984 ; Newman et al., 1984 ; Reinity and Turekian, 1991 ; Hémond et al., 1994) and more recent mass spectrometric studies using TIMS, SIMS and PIMMS (Cohen and O'Nions, 1993 ; Sims et al., 1995 ; 1999 ; Peitruszka, 2000). Most U-series studies have focused on the active shield-stage tholeiitic volcanoes- Kilauea and Mauna Loa (Krishnaswami, 1984 ; Newman et al., 1984 ; Reinitz and Turekian, 1991 ; Cohen et al., 1993 ; Hémond et al., 1994 ; Pietruszka, 2000). However, U-Th-Ra and U-Pa disequilibria have also been measured in young tholeiitic and alkaline lavas from the preshield-stage submarine volcano Loihi (Sims et al., 1995 ; 1999 ; Pietruszka, submitted ?) and alkaline

lavas from the post-shield stage volcanoes- Hualalai, and Mauna Kea and rejuvenated stage volcano- Haleakala (Sims et al. 1995 ; 1999). U-Th disequilibria have also been measured in young (or not quite so young) alkaline submarine flows from the South Arch (Sims et al. 1995).

The early U- and Th – series measurements, utilizing radioactive counting techniques, demonstated the existence of of significant radioactive disequilibria in lavas from Kilauea, suggesting that chemical fractionation between U-Th and Th-Ra occured during the formation of the Kilauean magmas, on a time scale of less than 350 ka and 8 ka, respectively. However, the origin of this fractionation- melting or secondary processs, such as assimilation of altered oceanic crust- was highly uncertain (Krishnaswami 1984). In a subsequent alpha counting study, Reinitz and Turekian (1991) measured the activities of several U-series nuclides in a suite of lavas erupted during the first two years of the ongoing Pu' O'o eruption (from 1983 to present). Their results confirmed the excess of ^{230}Th over ^{238}U, but more importantly demonstrated that the activity of ^{230}Th was correlated with the lavas incompatible trace element ratios, suggesting that partial melting was responsible for the fractionation of U from Th.

Recent mass spectrometric studies have consistently demonstrated that the ^{230}Th excesses in tholeiitic lavas from Loihi, Kilauea, and Mauna Loa are small (2 to 6% excesses) compared to the large ^{230}Th excesses seen in MORB (up to 25%), which are also mostly tholeiites. The ^{230}Th excesses in the Hawaiian tholeiites are relatively small (Cohen et al., 1993 ; Hémond et al. 1994 ; Sims et al. 1995 ; 1999 ; Pietruszka 2001) and constant (Pietruszka et al. 2000) , whereas the young alkalic lavas from the post-shield stage volcanoes- Hualalai, and Mauna Kea and rejuvenated stage volcano- Haleakala have much larger ^{230}Th excesses, from 15 to 30% (Sims et al. 1995 ; 1999). Furthermore, these ^{230}Th

excesses vary systematically across the range of compositions observed for Hawaiian lavas, with the smallest excess observed in the tholeiitic lavas and the largest excesses seen in the basanitic lavas from Haleakala.. This observation that $^{230}Th/^{238}U$ disequilibria in Hawaiian lavas are correlated with the lavas extent of melting, as inferred by its trace-and major-element chemistry, provides further evidence that U-Th fractionation is related to the melting process (Sims et al., 1995 ; 1999). In contrast to ($^{230}Th/^{238}U$), ($^{226}Ra/^{230}Th$) disequilibria in the the shield stage tholeiitic lava samples are much larger, with excesses ranging from 7 to 15% (Cohen et al. 1993 ; Hémond et al. 1994 ; Sims et al. 1999 ; Pietruszka et al. 2000 ; Cooper et al. 2001). For the alkalic lavas from Hualalai and Haleakala ^{226}Ra excesses are even larger, up to 30% (Sims et al. 1999). ($^{231}Pa/^{235}U$) in Hawaiian lavas (Pickett and Murrell 1997; Sims et al. 1999) shows the largest extents of parent –daughter fractionation with ^{231}Pa excesses ranging from 10 to 15% for the tholeitic lavas fom Kilauea, Mauna Loa and Loihi, up to 78% for the basanitic lavas from Halekala. Like ($^{230}Th/^{238}U$) the magnitude of the $^{231}Pa/^{235}U$ disequilibria, is related to the lavas major-element and trace-element chemistry, and by inference melt fraction. The relative extent of U-Th-Ra and U-Pa disequilibria observed in the Hawaiian lavas suggest that during melting of $D_{Ra} < D_{Th} < D_U$ and $D_{Pa} < D_U$. The observation that ($^{230}Th/^{238}U$) is greater than one in all Hawaiian lavas requires melting to be deep and most likely in the presence of garnet.

While it can be shown that the ^{238}U-^{230}Th and ^{235}U-^{231}Pa disequilibria are mainly sensitive to melt fraction because of the long half-lives of ^{230}Th and ^{231}Pa ((Sims et al. 1995 ; 1999 ; Elliott 1997) interpretation of ^{226}Ra data, because of its much shorter half-life, requires models that treat explicitly the time-scales of melt generation and melt extraction (e.g., McKenzie 1985; Spiegelman and Elliott 1993). Using a forward modeling approach to compare their data with the dynamic melting formalism of McKenzie (1984), Cohen et al. 1993 and Hémond et al. 1994 showed that measurements of ^{238}U–^{230}Th–^{226}Ra disequilibria in

tholeiiitc lavas from Kilauea and Mauna Loa can provide previously unattainable estimates of porosity (<1%), solid mantle upwelling rate (~10^{-3} kg $m^{-3}.a^{-1}$) and melt transport times (< 1.7 ka) beneath these volcanos. Using a similar forward modeling approach, Sims et al., showed that both chromatographic porous flow and dynamic melting of a garnet peridotite source can adequately explain the ^{238}U–^{230}Th–^{226}Ra and ^{235}U–^{231}Pa disequilibria in their suite of tholeiitic–to–basanitic lavas, but that in both cases the range in allowable melting conditions was highly dependent on the U-Th and (to a lesser extent) Ra and Pa partition coefficents. Using the observed range of experimental partition coefficients for U and Th (Beattie, 1993a,b; La Tourrette 1993; Lundstrom et al. 1994; Salters and Longhi, 1999.), they found that for chromatographic porous flow, the calculated maximum porosity in the melting zone ranges from 0.3–3% for tholeiites and 0.1–1% for alkali basalts and basanites, and solid mantle upwelling rates range from 40 to 100 $cm.yr^{-1}$ for tholeiites and from 1 to 3 $cm.yr^{-1}$ for basanites. For dynamic melting, the escape or threshold porosity is 0.5–2 % for tholeiites and 0.1–0.8% for alkali basalts and basanites, and solid mantle upwelling rates range from 10 to 30 $cm.yr^{-1}$ for tholeiites and from 0.1 to 1 $cm.yr^{-1}$ for basanites. While it is clear that the Hawaiian U-series data do not distinguish the mode of melting beneath Hawaii- dynamic or chromatographic- both models show that there is a significant range in the predicted solid mantle upwelling rates in the different volcanoes that extend from the leading edge to the trailing edge of the Hawaiian plume

Despite considerable evidence for the existence of a deep rooted mantle plume beneath Hawaii and numerous geochemical studies, including several measurements of U-series disequilibria, there have been very few studies constraining the nature of the melting region and the dynamics of the plume by combining geophysical and geochemical observations. Watson and Mckenzie (1991) used an axisymmetric plume model to calculate the melt production rate and bulk major and trace element chemistry of magmas resulting from an

axisymetric plume model. However, they did not try to account for the spatial and compositional variability seen in the chemistry of the erupted lavas , nor, did they try to take into account the effect of the overriding Pacific plate on the Hawaiian plume dynamics. Richardson and Mckenzie (1994) used the plume models developed by Watson and McKenzie (1991) to calculate the effects of an upwelling plume on U-series disequilibria, and to use these results to determine the melting rate (related to solid mantle upwelling rate) and porosity of the melting region. However, because there was very little U-series data from volcanoes other than Kilauea and Mauna Loa, they made no attempt to correlate spatial variability in the U-series activity ratios along the plume track with the dynamics of the plume. More recent work of Sims et al. (1999) which looked at U-series in young lavas extending from the center of the inferred Hawaiian plume out to its fringes, has shown that that solid mantle upwelling rates are highest in the plume center and lowest at its leading and trailing edges (Figure 13). These U-series upwelling rates are comparable to upwelling velocities calculated from the axis symmetric plume models of Watson and McKenzie (1991) and Hauri (1994), however, these U-series upwelling rates also show an asymmetry not predicted by these plume models. The observation that the solid mantle upwelling is greater for Loihi, than Hualalai and Haleakala appears to be more consistent with the recent plume model of Ribe and Christensen (1999) which takes into account the influence of the overriding Pacific plate on the plumes upwelling dynamics.

Figure Captions

Figure 1

Solidus in a P-T diagram for a dry peridotite, a wet peridotite, a pyroxenite and an eclogite. This diagram illustrates the range in solidus temperatures potentially found in the intraplate tectonic setting where compositional differences and differences in volatile contents are expected compared with the mid-ocean ridge (dry peridotite).

Figure 2

Schematic diagram of the top section of a mantle plume emphasizing the parameters involved in melting at hotspots. Solid lines indicates the flow lines for the solid mantle while the dashed lines indicates melt trajectories (adapted from Ribe and Smooke 1987). The size of the melting region is a function of the mantle temperature relative to ambient mantle, the amount of cooling of the overlying lithosphere and the width of the upwelling. Melting can also be influenced by heterogeneities that can modifiy solidus pressures and melting rates. The amount of melting produced per unit of time depends on the mantle upwelling velocity and is thus expected to be smaller on the edges of the plume. Some melting of the lithosphere can take place once the plume has heated the lithosphere. See text for more details.

Figure 3

Potential fractionation in U-series due to batch melting of: (a) garnet peridotite compared with amphibole bearing garnet peridotite. The mode of amphibole in the garnet-lherzolite is labeled on the melting curves (b) lherzolite at a range of pressures of melting. The model curves are labeled with pressures in GPa (c) mafic composition: garnet pyroxenite, eclogite, and websterite. The model curves were calculated using the partition coefficients of Landwehr et al. (2001) and Hauri et al. (1994) for pyroxenites and LaTourrette et al. (1995) for

amphibole. The model of Blundy and Wood (1994) was then used to estimate partition coefficients for Ra. As had been argued by Stracke et al. (2000), the mafic compositions do not produce large $^{230}Th/^{238}U$ fractionation because of the dominance of clinopyroxene.

Figure 4

($^{230}Th/^{238}U$) versus $\delta_{(Sm/Nd)}$, $\delta_{(Lu/Hf)}$, and $^{176}Hf/^{177}Hf$. $\delta_{(Lu/Hf)}$ is an indicator of the amount of residual garnet, whereas $\delta_{(Sm/Nd)}$ is an indicator of the degree of melting. For the Hawaiian basalts, the highest degree melts (low $\delta_{(Sm/Nd)}$) with the least prominent garnet signature (low $\delta_{(Lu/Hf)}$) are the most enriched melts (low $^{176}Hf/^{177}Hf$) with the lowest ^{230}Th-excesses. Curves are mixing lines between high degree garnet-pyroxenite and low degree garnet-peridotite derived melts. Degree of melting (F) for each endmember is indicated at the end of the curve, tick marks are for 10% mixing intervals. Solid circles are the Hawaiian data from this study. Shaded areas are the expected melting trends for a garnet-pyroxenite bearing source. All melting calculations are done by incremental batch melting with small melt increments (0.1%) and similar porosities (0.1%), i.e. dynamic melting. The trace element composition for the garnet-pyroxenite component is similar to depleted mid ocean ridge basalts (N-MORB), and the trace element composition of the garnet-peridotite is similar to MORB–source mantle (according to the geochemical earth reference model (GERM). Melt transport times are equal for both melting of garnet-pyroxenite and garnet-peridotite (mantle matrix ascent rates are 1cm/yr and melt ascent rates are 400cm/yr). Further explanations and sources of partition coefficients are given in the text.

Figure 5

Histogram Th/U for clinopyroxenes in peridotites and pyroxenites from the Ronda peridotite massif. Concentrations were measured by isotope dilution mass spectrometry in acid-leached clinopyroxenes. This histogram shows that pyroxenites do not have larger Th/U ratios than peridotites. Thus, the correlation found between $^{230}Th/^{238}U$ and Th/U cannot be explained by mixing of peridotite and pyroxenite melts as advocated in Sigmarsson et al. (1998). Data from Hauri et al. (1994) and Bourdon and Zindler (unpublished).

Figure 6

Nb/U versus $^{230}Th/^{238}U$ diagram to illustrate the effect of accessory phases (e.g. rutile) on trace element fractionation in OIB. It is generally found that Nb/U ratio show a relatively restricted range in ocean island basalts (Hofmann, 1986) except when there is evidence for sediment recycling in their source (Sims and DePaolo 1997). The data for Lanzarote are shown here for reference (Sigmarsson et al. 1998; Carracedo et al. 1990). The curve is a batch melting curve of a rutile-bearing pyroxenite with the mode of rutile estimated such that $^{230}Th/^{238}U$ matches observed values (X^{rutile}=0.01). The partition coefficients used in this calculation are as follows: D_U^{garnet}=0.04, D_U^{cpx}=0.01, D_{Nb}^{rutile}=29. If rutile was present as a residual phase in the source ocean island basalts, it would have a dramatic effect on their Nb/U ratios, in contrast with what is observed.

Figure 7

$^{230}Th/^{232}Th$ versus $^{87}Sr/^{86}Sr$ diagram for mid-ocean ridge, ocean island and continental basalts compiled from the literature (Turner et al. 1997; Bourdon et al. 1996; Dosso et al. 1999; Claude-Ivanaj et al. 1998, 2001; Bourdon et al. 1998; Sims et al. 1995, 1999; Reid and Ramos 1996; Sigmarsson et al. 1998; Williams et al. 1992; Asmerom and Edwards 1995; Asmerom 1999; Thomas et al. 1999 and unpublished data from Sims and Hart, and Bourdon and

Turner). This new data set based on mass spectrometry data shows a hyperbolic rather than a linear trend. If this is interpreted as reflecting a mixing line, this indicates that the Th/Sr ratios in the enriched components (low $^{230}Th/^{232}Th$ ratios) is greater than the Th/Sr ratio in the depleted component. The lavas (in particular continental basalts from the Great Rift) must have had a distinct evolution and can be explained by a recent metasomatism of the lithosphere (see text).

Figure 8

$^{208}Pb^*/^{206}Pb^*$ versus Th/U diagram for mid-ocean ridge and ocean island basalt based on a recent data set with mostly mass spectrometry measurements (Turner et al. 1997; Bourdon et al. 1996; Dosso et al. 1999; Claude-Ivanaj et al. 1998, 2001). The data shows a relatively well defined array that intersect a closed-system line for the bulk Earth starting with an initial lead isotope composition equal to Canyon Diablo (T=4.55 Ga). This intersect was used by Allègre et al. (1986) to define the Th/U ratio of the Earth.

Figure 9

Comparison of the measured ($^{226}Ra/^{230}Th$) and ($^{230}Th/^{238}U$) for the Hawaiian basalts (symbols) to the calculated values (curves) for a) chromatographic melting (Spiegelman and Elliott, 1993) and b) dynamic melting (Mckenzie, 1985) through a 1D melt column. using the partition coefficients of La Tourrette et al. Data are a compilation of mass spectrometric measurements from Cohen et al., 1994; Sims et al., 1995; 1999; Pietruszka et al., 2000) For chromatographic melting- the results are calculated for a 50 km melt column and the horizontally trending curves show activity ratios for constant maximum porosity (ϕ_{max}) in

percent, while the vertically trending contours show the activity ratios for a constant upwelling rate (W_S) in cm/yr. For dynamic melting the horizontally trending curves show activity ratios for constant threshold porosity (ϕ_{thres}) in percent, while the vertically trending contours show the activity ratios for a constant upwelling rate (W_S) in cm/yr. In both plots, the bold solid contour shows a reference upwelling rate of 10 cm/yr, while the bold dashed curve shows a reference porosity of about 1% (phi max for chromatographic melting and phi critical for dynamic melting). Spacing between curves is calculated in log units: increments between curves of solid upwelling rate are $10^{0.2}$ cm/yr, and between curves of constant maximum porosity $10^{0.13}$ %. Note that with chromatographic melting the decrease of (^{230}Th/^{238}U)at very low upwelling rates is a result of the melting rate approaching the time-scale of the half-life of ^{230}Th. Error bars for (^{226}Ra/^{230}Th) reflect the uncertainties in ^{14}C ages (see Sims et al., 1999).

Figure 10

Comparison of the measured (^{231}Pa/^{235}U) and (^{230}Th/^{238}U) for Hawaiian basalts (Sims et al. 1999) to the calculated values (curves) for a) chromatographic melting (Spiegelman and Elliott, 1993) and b) dynamic melting (Mckenzie, 1985) through a 1D melt column. using the partition coefficients of La Tourrette et al. For chromatographic melting- the results are calculated for a 50 km melt column and the horizontally trending curves show activity ratios for constant maximum porosity (ϕ_{max}) in percent, while the vertically trending contours show the activity ratios for a constant upwelling rate (W_S) in cm/yr. For dynamic melting the horizontally trending curves show activity ratios for constant threshold porosity (ϕ_{thres}) in percent, while the vertically trending contours show the activity ratios for a constant upwelling rate (W_S) in cm/yr. In both plots, the bold solid contour shows a reference

upwelling rate of 10cm/yr, while the bold dashed curve shows a reference porosity of about 1% (phi max for chromatographic melting and phi critical for dynamic melting). Spacing between curves is calculated in log units: increments between curves of solid upwelling rate are $10^{0.2}$ cm/yr, and between curves of constant maximum porosity $10^{0.13}$ %. The decrease of (^{231}Pa/^{238}U) and (^{230}Th/^{238}U) at very low upwelling rates is a result of the melting rate approaching the time-scale of the half-lives of ^{231}Pa and ^{230}Th.

Figure 11

^{230}Th-^{238}U isochron diagram for for mid-ocean ridge, ocean island and continental basalts compiled from the literature (references indicates in the caption of Fig. 7 and unpublished data from Sims and Hart, and Bourdon and Turner). All the lavas plot to the left of the equiline where the activity of ^{230}Th is equal to the activity of ^{238}U. This indicates that the OIB lavas are generated by melting of a source containing high-pressure clinopyroxene or garnet (see text).

Figure 12

Compilation of ^{230}Th-^{238}U and ^{231}Pa-^{235}U activity ratios for ocean island basalts and mid-ocean ridge basalts (Pickett et al. 1997; Lundstrom et al. 1998, Bourdon et al 1998; Sims et al. 1999; Vigier et al. 1999; Bourdon and Turner, in prep). The data show two clearly distinct linear trends. The model curves for melting a lherzolite at various pressures (taken from Figure 4) are also shown for reference and show that the OIB trend can be generated by melting at an initial pressure of melting greater than for MORB. This is a clear indication of the influence of garnet on the ^{230}Th-^{238}U fractionation in OIB. As advocated by Pickett and Murrell (1997), ^{231}Pa-^{235}U fractionation can be produced by clinopyroxene and does not require garnet as a residual phase.

Figure 13

Solid mantle upwelling rate calculated from ^{238}U-^{230}Th-^{226}Ra and ^{235}U-^{231}Pa disequilibria versus the radial position of the volcanoes relative to the center of the Hawaiian plume. The center of the plume (see inset) is located so that the active volcanoes Loihi, Kilauea and Mauna Loa are positioned appropriately for their model ages and eruption rates (DePaolo and Stolper, 1996). Also shown are the model curves for solid mantle upwelling from Watson and McKenzie (1991) and Hauri et al. (1994). The model of Watson and McKenzie (1991) assumes a constant viscosity across the plume whereas the Hauri et al. model incorporates a temperature-dependent viscosity. The values inferred from the U-series data are reasonably consistent with the Watson and McKenzie (1991) model near the fringes of the plume and considerably lower than the Hauri et al. (1994) model values. For Kilauea and Mauna Loa, the inferred upwelling velocities are probably representative of the core of the plume, and these are also closer to the Watson and McKenzie (1991) values than they are to the Hauri et al. (1994) model values. These estimates will need to be refined with more accurate values of distribution coefficients and better models for the melt productivity, but they illustrate that the U-series disequilibrium isotopic data may provide a much-needed constraint on the dynamics of the plume.

Appendix: Analytical solutions for time dependent melting models

A. Dynamic Melt Transport

Analytical solutions for ^{238}U-^{230}Th-^{236}Ra disequilibria during dynamic melting (near fractional) were first derived by McKenzie (1985) and have subsequently been presented in several papers pertaining to the production of U-series disequilibria in basaltic melts (Williams and Gill, 1989; Beattie, 1993a; Chabaux and Allègre, 1994; Sims et al., 1999).

Assuming a constant melt rate (Γ), by mass, and porosity (ϕ), the ($^{230}Th/^{238}U$) and $^{226}Ra/^{230}Th$) can be expressed as a function of ϕ and Γ:

$$\left(\frac{^{230}Th}{^{238}U}\right) = \frac{F_{Th}(K_U + \lambda_{Th})}{F_U(K_{Th} + \lambda_{Th})} \tag{1}$$

$$\left(\frac{^{226}Ra}{^{230}Th}\right) = \frac{F_{Ra}(K_{Th} + \lambda_{Ra})}{F_{Th}(K_{Ra} + \lambda_{Ra})}\left\{1 + \frac{\lambda_{Th}(K_U - K_{Th})}{(K_{Th} + \lambda_{Ra})(K_U + \lambda_{Th}}\right\} \tag{2}$$

where

$$F_i = \frac{\phi\rho_f}{D_i\rho_s(1-\phi) + \phi\rho_f} \tag{3}$$

and

$$K_i = \frac{F_i(1-D_i)}{\phi\rho_f}\Gamma_0 \tag{4}$$

D_i is the bulk mineral/melt partition coefficient and ρ_f and ρ_s are the densities of the melt and peridotite (2800 and 3300 kgm^{-3}). A similar expression to equation 1 can be derived for ($^{231}Pa/^{235}U$).

B. Chromatographic Melt Transport.

Numeric solutions for ^{238}U-^{230}Th-^{236}Ra disequilibria during chromatographic melting were first derived by Spiegelman and Elliott, 1993 (note that there is a user form of this solution on User calc….). While Spiegelman and Elliott pointed out that the system of equations for the production of U-series disequilibria during chromatographic melting could be solved analytically, these expressions were never presented (and in fact, determining this solution from their paper is rather problematic given the typo in equation 15) Subsequent efforts by Sims (1995) showed that there was a simple analytical approximation for the chromatographic

melting expressions. These two solutions, which were originally presented in Sims et al., 1999, are given below along with a comparison between results obtained from analytical solutions and those obtained numerically.

Analytical Solutions

Following the approach of Spiegelman and Elliott (1993), the effects of transport of melt through a melting column on the chemistry of radiogenic isotopes can be separated from melting by expressing the concentration of an element as:

$$c_i = \alpha_i c_{bi} \tag{5}$$

Where c_i is the concentration of an element measured at the surface, c_{bi} is the concentration of a stable element due to batch melting and α_i is the enrichment factor due to transport. The concentrations in the melt are given by the batch melting equation, despite the fact that the porosity is small and the melt moves relative to the solid, because of the assumption of continuous re-equilibration of solid and liquid. Fractional melts are produced only if the solid does not re-equilibrate with the melt that passes through (see Appendix of Spiegelman and Elliot (1993)).

For the decay chain ^{238}U-^{230}Th-^{226}Ra, the change in a_i with position in a 1D melt column for each isotope can be expressed by the following (Note that in equation (15) of Spiegelman and Elliot (1993) there is a typographical error)

$$\frac{d\alpha_0}{d\zeta} = -\lambda_o \tau_0 \alpha_0 \tag{6}$$

$$\frac{d\alpha_1}{d\zeta} = \lambda_1(\tau_0\alpha_0 - \tau_1\alpha_1) \tag{7}$$

$$\frac{d\alpha_2}{d\zeta} = \lambda_2(\tau_1\alpha_1 - \tau_2\alpha_2) \tag{8}$$

Where ζ is the dimensionless distance *(z/d)* along a column of length *d*, λ_i are the decay constants (_n(2)/$t_{1/2}$), and $\tau_i = d/w^i_{eff}$ is the effective velocity is given by

$$w^i_{eff} = \frac{\rho_f \phi w + p_s(1-\phi)D_i W}{\rho_f \phi + p_s(1-\phi)D_i} \tag{9}$$

Where p_f and p_s are the melt and solid densiities, respectively, ϕ is the porosity, w is the melt velocity. W is the solid upwelling velocity and D_i is the bulk partition coefficient. Note that the if the partition coefficient D_i is <<1, the effective velocity approaches the melt velocity, and also that the difference in effective velocity between elements with different D_i decreases

at larger porosities. In the following text, the subscripts O, 1, and 2 are taken to refer to ^{238}U, ^{230}Th, and ^{226}Ra, respectively.

Equations (6-8) form a coupled system of differential equations, whereby the decay of each parent can increase the concentration of the daughter element as melt migrates through the melting region. To what these equations for the enrichment factor α_i, we can make the problem analytically tractable by assuming that both the melt velocity (w) and porosity (ϕ) remain constant over the melt column using only their average values. (It should be emphasized that the assumption of constant porosity is made with reference to the migration of melt only, and that for the purposes of melting of the solid matrix, the melt fraction at the solidus is zero and increases linearly upwards.) For a 1D steady-state melting column, the average melt velocity is given by

$$w = \frac{\Gamma d}{\rho_i \phi 2} \tag{10}$$

Where Γ is the melting rate, which we assume to be constant is given by

$$\Gamma = \frac{W \rho_s F_{\max}}{d} \tag{11}$$

Solving equations (6-8), we obtain

$$\alpha_0(\zeta) = \alpha_0^o e^{-\lambda_0 \tau_0 \zeta} \tag{12}$$

$$\alpha_1(\zeta) = \frac{\lambda_1 \tau_0 \alpha_0^o}{\lambda 1 \tau - \lambda_0 \tau_0} e^{-\lambda_0 \tau_0 \zeta} + \left[\alpha_1^o - \frac{\lambda_1 \tau 0 \alpha_0^o}{\lambda_1 \tau_1 - \lambda_0 \tau_0} \right] e^{-\lambda_1 \tau_1 \zeta} \tag{13}$$

$$\begin{aligned} \alpha_2(\zeta) = {} & \frac{\lambda_2 \lambda_1 \tau_1 \tau_0 \alpha_0^o}{(\lambda_1 \tau_1 - \lambda_0 \tau_0)(\lambda_2 \tau_2 - \lambda_0 \tau_0)} e^{-\lambda_0 \tau_0 \zeta} + \frac{\lambda_2 \tau_1}{\lambda_2 \tau_2 - \lambda_1 \tau_1} \left[\alpha_1^o - \frac{\lambda_1 \tau_0 \alpha_1^o}{\lambda_1 \tau_1 - \lambda_0 \tau_0} \right] e^{-\lambda_1 \tau_1 \zeta} \\ & + \left[\alpha_2^o - \frac{\lambda_2 \lambda_1 \tau_1 \tau_0 \alpha_0^o}{(\lambda_1 \tau_1 - \lambda_0 \tau_0)(\lambda_2 \tau_2 - \lambda_0 \tau_0)} - \frac{\lambda_2 \tau_1}{\lambda_2 \tau_2 - \lambda_1 \tau_1} \left(\alpha_1^o - \frac{\lambda_1 \tau 0 \alpha_0^o}{\lambda_1 \tau_1 - \lambda_0 \tau_0} \right) \right] e^{-\lambda_2 \tau_2 \zeta} \end{aligned} \tag{14}$$

Where α_0^o , α_1^o and α_2^o are constants of integration. For secular equilibrium at the base of the melting column, we set $\alpha_i^o = 1$.

Figure A1(a) shows the constant value of porosity used in the analytic model (dashed curve), compared to the porosity distribution for a 1D melt column in which the upward flux of melt is required to remain constant (see Spiegelman and Elliot, 1993). The solid curves in Figure A1(b) show values of α_i calculated from equations (12-14) along the (dimensionless) length of the melting column for the ^{238}U decay chain with a constant porosity of .1% and solid upwelling velocity of 1 cm/yr.

As has been shown by Sims (1995) and Sims et al., (1999) an analytical approximation to chromatographic melting can also be obtained by solving equations (7) and (8) while holding the values of α_o and α_i held constant, respectively.

$$\alpha_0(\zeta) = \alpha_0^o e^{-\lambda_0 \tau_0 \zeta} \tag{15}$$

$$\alpha_1(\zeta) = \alpha_1^o e^{-\lambda_1 \tau_1 \zeta} + \frac{\tau_0}{\tau_1}\alpha_0\left[1 - e^{-\lambda_1 \tau_1 \zeta}\right] \tag{16}$$

$$\alpha_2(\zeta) = \alpha_2^o e^{-\lambda_2 \tau_2 \zeta} + \frac{\tau_1}{\tau_2}\alpha_1\left[1 - e^{-\lambda_2 \tau_2 \zeta}\right] \tag{17}$$

Holding the values of α_o and α_i constant is equivalent to saying that the change in α for a given daughter isotope over the melt column is large compared to that of the parent element. It is evident in Figure A1(b) shows that this approximate analytical solution (dashed curves) is nearly identical to the full analytic solution. The reason for this can be seen by considering the terms $\lambda_o\tau_o$, $\lambda_1\tau_1$, and $\lambda_2\tau_2$, in the full analytic solution (equations 12-14), which represent the ratio of the effective transport time with the time taken for concentration of the isotope to decrease by half. For ^{238}U, $e^{-\lambda 0 \tau 0 \zeta} \approx 1$, while for ^{226}Ra, $e^{-\lambda 2 \tau 2 \zeta} \approx 0$. With these approximations, α_1 in equations (13) and (16) are identical, and this is evident in Figure A1(b). For α_2, equation (14) reduces to equation (17) if $\lambda_1\tau_1 << \lambda_2\tau_2$, which is nearly true for ^{230}Th and ^{226}Ra. Therefore, for the ^{238}U decay chain, the system of ordinary differential equations (6-8) can essentially be treated as if they are decoupled.

Comparison of Analytical Solutions with the full Numerical Solution

Figure A1(c) shows the full numerical solution for α of Spiegelman and Elliot (1993). It is evident that in comparison of A1(c) with A1(b), the numerical and analytic solutions differ significantly, with the analytic solution overestimating ($^{226}Ra/^{230}Th$). In Figure A2, comparison of the activity ratios calculated from the full analytic solution (light solid curves), the approximate analytic solution (light dotted curves), and the full numerical solution (dark solid curves) is shown for ($^{226}Ra/^{230}Th$) and $^{230}Th/^{238}U$) using a melt column of 50 km and total melt fraction of 15% and constant partition coefficients from Lundstrom et al. (1994) for garnet peridotite. The maximum porosity for the melt column is varied from 0.1-10% and the solid upwelling velocity is varied from 1-100 cm/yr. It is clear that there is a major difference between the analytic and numerical solutions. Considering that ($^{226}Ra/^{230}Th$) is controlled mainly by the porosity, while ($^{230}Th/^{238}U$) is controlled mainly by the upwelling rate, it can be concluded that the analytic solution overestimates the porosity and under-estimates the upwelling velocity.

From the results in Figure A2, it is not clear that the analytic solutions using the average porosity and melt velocity do a very good job at approximating the numerical solution. Both the ($^{226}Ra/^{230}Th$) and ($^{230}Th/^{238}U$) values are significantly different from the numerical solution, indicating the importance of taking into consideration the details of the porosity distribution and melt velocity along the melt column. However, because these analytical solutions, pariticularily the analytical approximation, can be easily calculated with MATLAB scripts or in excel type spreadsheets, these solutions can be broken into discrete

increments of the melt column with the total results summed over the whole melt column. This allows the analytical approximation to used in models which have discrete multiple porosities.

C. Box-model for equilibrium melting:

In what follows, we present a simplified box-model that capture the essential of the chromatographic porous flow model with the only assumption that there is equilibration between the melt and the matrix. If one assumes that the melting column is in steady-state, then the following mass balance equations for U and Th can be written:

$$M_c \frac{dU_c}{dt} = \dot{M}_i U_i - \dot{M}_m U_m - \dot{M}_s U_s \qquad (18)$$

where m denotes the melt, s the solid and i the material input at the base of the melting column. The dotted parameters are mass fluxes. The corresponding equation for Th (or Pa) would be:

$$M_c \frac{dTh_c}{dt} = \dot{M}_i Th_i - \dot{M}_m Th_m - \dot{M}_s Th_s - \lambda_{Th} M_c Th_c + \lambda_U M_c U_c \qquad (19)$$

At steady-state, the left-hand side of the equation disappears and the equations can be simplified if one makes the assumption that melt is in equilibrium with the solid at the top of the melting column:

$$D_{Th} = \frac{Th_s}{Th_m} \qquad \text{and} \qquad D_U = \frac{U_s}{U_m}$$

Then, the degree of melting for the solid at the top of the melt column is:

$$F = \frac{\dot{M}_m}{\dot{M}_i} \qquad (20)$$

The equations (1) and (2) can be combined:

$$\frac{Th_i}{U_i} = \frac{Th_m}{U_m}\left[F.\frac{U_m}{U_i} + (1-F)\frac{U_m}{U_i}.\frac{D_{Th}}{D_U}\right] - \frac{M_c}{\dot{M}_i}.\frac{U_m}{U_i}\left[\lambda_U - \lambda_{Th}\frac{Th_m}{U_m}\right] \qquad (21)$$

If we assume that the material coming in the box is in secular equilibrium, this equation can be further simplified and multiplied by λ_{Th}/λ_U to yield activity ratios:

$$1 = \left(\frac{Th}{U}\right)_m\left[\frac{F + D_{Th}(1-F)}{F + D_U(1-F)}\right] - \lambda_{Th}\frac{M_c}{\dot{M}_i}.\left[\frac{U_c}{\dot{U}_i} - \frac{Th_c}{\dot{Th}_i}\right] \qquad (22)$$

If one expresses the Th/U activity ratio in the melt:

$$\left(\frac{Th}{U}\right)_m = \left[\frac{F + D_U(1-F)}{F + D_{Th}(1-F)}\right].\left(1 + \lambda_{Th}.\left[\tau_U - \tau_{Th}\right]\right) \qquad (23)$$

where τ_U and τ_{Th} are the residence times U and Th respectively in the melting column. The residence times can be expressed as follows:

$$\tau_U = \frac{M_c U_c}{\dot{M}_i U_i} \qquad (24)$$

In the equation (6), the first term of the right-hand side correspond to a batch melting model and the second term correspond to an in-growth term due to a longer residence time of U relative to Th. This equation is identical to the equation (31) in Spiegelman and Elliott in their appendix A.4. It is obtained with a much simpler derivation and no assumption about melt transport. Our approach highlights that in the case of equilibrium melting, the fractionation between short-lived isotopes is simply dependent on the relative residence time of the elements in the melting column that comes out of a simple box model and the half-life of the daughter nuclide.

Figure Captions

Figure A1: a) Porosity distribution (f) for a 1D melt column (solid curve) assuming constant melt flux (see Spiegelman and Elliot, 1993). Average porosity is shown as the dashed line. b) Enrichment factors (a) calculated from the analytical solution (solid curves) and approximate analytical solution (dotted curves) for ^{238}U, ^{230}Th and ^{226}Ra. c) Enrichment factors (a) calculated from the numerical solution of Spiegelman and Elliot(1993) for ^{238}U, ^{230}Th and ^{226}Ra. In these plots depth (z) is non-dimensionalized. See text for explanation.

Figure A2:($^{226}Ra/^{230}Th$) and ($^{230}Th/^{238}U$) calculated from the analytical solution (solid light curves), approximate analytical solution (dotted light curves) and full numerical solution (solid dark curves). Horizontal curves represent constant maximum porosity (f_{max}), while vertical curves represent constant upwelling rates (W_s) in cm/yr. Selected contours are labeled. Contours range from 1-100 cm/yr and 0.1-10% for upwelling velocity and maximum porosity, respectively. See text for explanation.

References :

Allègre CJ, Condomines M (1982) Basalt genesis and mantle structure studied through Th-isotopic geochemistry. Nature 299: 21-24

Allègre CJ, Turcotte D (1986) Implications of a two-component marble-cake mantle. Nature 323: 123-127

Asimow PD, Hirschmann MM, Ghiorso MS, O'Hara MJ Stolper EM (1995) The effect of pressure-induced solid-solid phase transitions on decompression melting of the mantle. Geochim Cosmochim Acta, 59: 4489-4506

Asmerom Y(1999) Th-U fractionation and mantle structure. Earth Planet Sci Lett 166: 163-175

Asmerom Y, Edwards R L (1995) U-series isotope evidence for the origin of continental basalts. Earth Planet Sci Lett 134: 1-7

Asmerom Y, Cheng H, Thomas R, Hirschmann M, Edwards RL (2000) Melting of the Earth's lithospheric mantle inferred from protactinium-thorium-uranium isotopic data. Nature 406: 293-296

Baker MB, Hirschmann MM, Ghiorso MS, Stolper EM (1995) Compositions of near-solidus peridotite melts from experiments and thermodynamic calculations. Nature 375: 308-311

Beattie PD (1993) Uranium-thorium disequilibria and partitioning on melting of garnet peridotite. Nature 363: 63-65

Bercovici D, Lin J (1996) A gravity current model of cooling mantle plume heads with temperature dependent buoyancy and viscosity. J Geophys Res 101: 3291-3309

Blundy J, Wood B (1994) Prediction of crystal-melt partition coefficients from elastic moduli. Nature 372: 452-454

Bourdon B, Langmuir C, Zindler A (1996) Rigde-hotspot interaction along the Mid-Atlantic ridge between 37°30 and 40°30 N: the U-Th disequilibrium evidence. Earth Planet Sci Lett 142: 175-196

Bourdon B, Joron J-L, Claude-Ivanaj C, Allègre CJ (1998) U-Th-Pa-Ra systematics for the Grande Comore volcanics: melting processes in an upwelling plume. Earth Planet Sci Lett 164: 119-133

Bourdon B and Turner SP (in prep) Upwelling rates beneath hotspots : evidence from U-series in basalts from the Azores region.

Carracedo JC, Badiola ER, Soler V (1990) Aspectos volcanologicos y estructurales, evolucion opetrologica e implicaciones en riesgo volcanico de la erupcion de 1730 en Lanzarote, Islas Canarias. Estud Geol 46: 25-55

Chabaux F, Allègre CJ (1994) ^{238}U-^{230}Th-^{226}Ra disequilibria in volcanics- a new insight into melting conditions. Earth Planet Sci Lett 126: 61-74

Chen C-Y Frey, F.A (1985) Trace element and isotopic geochemistry of lavas from Haleakala volcano, East Maui, Hawaii; implications for the origins of Hawaiian basalts. J. Geophys Res 90: 8743-8768

Class C, Goldstein SL, Altherr R, Bachèlery P (1998) The process of plume-lithosphere interactions in the ocean basins- the case of Grande Comore. J Pet 39: 881-903

Class C, Goldstein SL (1997) Plume-lithosphere interaction in the ocean basins: constraints from the source mineralogy. Earth Planet Sci Lett 150: 245-260

Claude-Ivanaj C, Bourdon B, Allègre CJ (1998) Ra-Th-Sr isotope systematics in Grande Comore Island: a case study of plume-lithosphere interaction. Earth Planet Sci Lett 164: 99-117

Claude-Ivanaj C, Joron J-L, Allègre CJ (2001) ^{238}U-^{230}Th-^{226}Ra fractionation in historical lavas from the Azores : long-lived source heterogeneity vs. Metasomatism fingerprints. Chem Geol 176: 295-310

Cohen AS, O'Nions RK (1993) Melting rates beneath Hawaii : evidence from uranium series isotopes in recent lavas. Earth Planet Sci Lett 120: 169-175

Cohen AS, O'Nions RK, Kurz MD (1996) Chemical and isotopic variations in Mauna Loa tholeiites. Earth Planet Sci Lett 143: 111-124

Cooper KM, Reid, Mary R, Murrell, MT; Clague, David A (2001) Crystal and magma residence at Kilauea Volcano, Hawaii; ^{230}Th- ^{226}Ra dating of the 1955 East Rift eruption. Earth Planet Sci Lett 184: 703-718

Condomines M, Hémond C, Allègre CJ (1988) U-Th-Ra radioactive disequilibria and magmatic processes. Earth Planet Sci Lett 90: 243-262

Condomines M, Sigmarsson O (2000) ^{238}U-^{230}Th disequilibria and mantle processes : a discussion. Chem Geol 162: 95-104

Dupré B, Lambret B, Allègre CJ (1982) Isotopic variations within a single oceanic island: the Terceira case. Nature 299: 620-622

Falloon TJ, Green DH (1989) The solidus of carbonated, fertile peridotite. Earth Planet Sci Lett 94: 364-370

Galer SJG, O'Nions RK (1986) Magmagenesis and the mapping of chemical and isotopic variations in the mantle. Chem Geol 56: 45-61

Gast PW (1968) Trace element fractionation and the origin of tholeiitic and alkaline magma type. Geochim Cosmochim Acta 32: 1057-1086

Griffiths RW (1986) The differing effects of compositional and thermal buoyancies on the evolution of mantle diapirs. Phys Earth Planet Inter 43: 261-273

Griffiths RW, Campbell IH (1991) On the dynamics of long-lived plume conduits in the convective mantle. Earth Planet Sci Lett 103: 214-222

Hart SR (1988) Heterogeneous mantle domains: signatures, genesis and mixing chronologies. Earth Planet Sci Lett 90: 273-296

Hauri EH, Whitehead JA, Hart SR, (1994) Fluid dynamic and geochemical aspects of entrainment in mantle plumes. J Geophys Res 99: 24,275-24,300.

Hawkesworth CJ, Kempton PD, Rogers NW, Ellam RM, van Calsteren PW (1990) Continental mantle lithosphere, and shallow level enrichment processes in the Earth's mantle. Earth Planet Sci Lett 96: 256-268

Hémond C, Condomines M, Fourcade S, Allègre CJ, Oskarsson N, Javoy M (1988) Thorium, strontium and oxygen isotopic geochemistry in recent tholeiites from Iceland : crustal influence on mantle-derived magmas. Earth Planet Sci Lett 87: 273-285

Hémond C, Hofmann AW, Heusser G, Condomines M, Rhodes JM, Garcia MO (1994) U-Th-Ra systematics in Kilauea and Mauna Loa basalts, Contrib Mineral Petrol 116: 163-180

Hirose K (1997) Partial melt compositions of carbonated peridotite at 3 GPa and role of CO_2 in alkali basalt magma generation. Geophys Res Lett 24: 2837-2840

Hirschmann MM, Stolper EM (1996) A possible role for pyroxenite in the origin of the garnet signature in MORB, Contrib Mineral Petrol 124: 185-208

Hirschmann MM, Asimow PD, Ghiorso MS, Stolper EM (199) Calculation of peridotite partial melting form thermodynamic model of minerals and melts III. Controls on isobaric melt production and the effect of water on melt production. J Petrol. 40: 831-851

Hirth G Kolhstedt DL (1996) Water in the oceanic upper mantle : implications for rheology, melt extraction and the evolution of the lithosphere. Earth Planet Sci Lett 144: 93-108

Hoernle K, Gill J, Schmincke HU (1993) Extreme fractionation of (Nb, K, Th)/U ratios during metasomatism of Jurassic oceanic lithospheric mantle. Eos Trans Am Geophys U 74: 633 1993

Huang Y, Hawkesworth C, Carlsteren Pv, Smith I, Black P (1997) Melt generation models for the Auckland volcanic field, New Zealand: constraints from U-Th isotopes. Earth Planet Sci Lett 149: 67-84

Ito G, Shen Y, Hirth G, Wolfe CJ (1999) Mantle flow, melting, and dehydration of the Iceland mantle plume. Earth Planet Sci Lett 165: 81-96

Kushiro I (1968) Compositions of magmas formed by partial zone melting of the Earth's upper mantle. J Geophys Res 73: 619-634

Landwehr D, Blundy J, Chamorro-Perez E, Hill E, Wood B (2001) U-series disequilibria generated by partial melting of spinel lherzolite. Earth Planet Sci Lett 188: 329-348

Langmuir CH, Hanson GN (1980) An evaluation of major element heterogeneity in the mantle sources of basalts. Phil Trans R Soc London A 297: 383-407

Lassiter JC, Hauri EH (1998) Osmium-isotope variations in Hawaiian lavas: evidence for recycled oceanic lithosphere in the Hawaiian plume. Earth Planet Sci Lett 164: 483-496

LaTourrette TZ, Kennedy AK, Wasserburg GJ (1993) Thorium-uranium fractionation by garnet: evidence for a deep source and rapid rise of oceanic basalts. Science 261: 739-742

Liu M, Chase CG (1991) Evolution of Hawaiian basalts: a hotspot melting model. Earth Planet Sci Lett 104: 151-165

Loper DE, Stacey FD (1983) The dynamical and thermal structure of deep mantle plume. Phys. Earth Planet Int 33: 304-317

Lundstrom CC, Shaw HF, Ryerson FJ, Phinney DL, Gill JB, Williams Q (1994) Compositional controls on the partitioning of U, TH, Ba, Pb, Sr and Zr between clinopyroxene and haplobasaltic melts: implications for uranium series disequilibria in basalts. Earth Planet Sci Lett 128: 407-423

MacDonald GA, Katsura T (1964) Chemical composition of Hawaiian lavas. J Petrol 5: 82-133

McKenzie D (1985) ^{230}Th-^{238}U disequilibrium and the melting processes beneath ridge; Earth Planet Sci Lett 72: 149-157

McKenzie (1989) Some remarks on the movement of small melt fractions in the mantle. Earth Planet Sci Lett 95: 53-72

Minster JF, Allègre CJ (1978) Systematic use of trace elements in igneous processes. Part III: Inverse problem of batch melting in volcanic suites. Contrib Mineral Petrol 68: 37-52

Morgan JW (1971) Convection plumes in the lower mantle. Nature 230: 42-43

Newman S., Finkel R.C. Macdougall J.D. (1984) Comparison of ^{230}Th-^{238}U disequilibrium systematics in lavas from three hot spot regions : Hawaii, Prince Edward and Samoa, Geochim. Cosmochim. Acta, 48, 315-324.

Olafsson M, Eggler DH (1983) Phase relations of amphibole, amphibole-carbonate, and phlogopite-carbonate peridotite: petrologic constraints on the asthenosphere. Earth Planet Sci Lett 64: 305-315

Olson P, Schubert G, Anderson C, Goldman P (1988) Plume formation and lithosphere erosion : a comparison of laboratory and numerical experiments, J. Geophys. Res. 93, 15 ,065-15,084.

Pearson DG, Shirey SB, Carlson RW, Boyd FR, Nixon PH (1995) Stabilisation of Archean lithospheric mantle: A Re-Os isotope isotope study of peridotite xenoliths. Earth Planet Sci Lett 134: 341-357

Pickett DA, MT Murrell (1997) Observations of $^{231}Pa/^{235}U$ disequilibrium in volcanic rocks. Earth Planet Sci Lett 148: 259-271

Pietruszka AJ, Rubin KH, Garcia MO (2000) ^{226}Ra-^{230}Th-^{238}U disequilibria of historical Kilauea lavas (1790-1982) and the dynamics of mantle melting within the Hawaiian plume; Earth Planet Sci Lett 186: 15-31

Rabinowicz M, Ceuleneer G, Monnereau M, Rosemberg C (1990) Three-dimensional models of mantle flow across a low-viscosity zone : implications for hotspot dynamics. Earth Planet Sci Lett 99: 170-184

Reid MR(1995) Processes of mantle enrichment and magmatic differentiation in the eastern Snake River Plain : Th isotope evidence. Earth Planet Sci Lett, 131: 239-254

Ribe NM (1988) Dynamical geochemistry of the Hawaiian plume. Earth Planet Sci Lett 88: 37-46

Ribe NM (1996) The dynamics of plume-ridge interaction 2. Off-ridge plumes. J. Geophys. Res. 101: 16,195-16,204

Ribe NM Smooke MD (1987) A stagnation point flow model for melt extraction from a mantle plume. J Geophys Res 92: 6437-6443

Ribe NM, Christensen UR (1999) The dynamical origin of Hawaiian volcanism. Earth Planet Sci Lett 171: 517-531

Schiano P, Bourdon B, Clochiatti R, Massare D, Varela ME, Bottinga Y (1998) Low-degree partial melting trends recorded in upper mantle minerals. Earth Planet Sci Lett 160: 537-550

Schilling JG (1973) Iceland mantle plume geochemical evidence along Reykjanes Ridge. Nature 242: 663-706

Schi!ling JG (1991) Fluxes and excess temperatures of mantle plumes inferred from their interaction with migrating mid-ocean ridges. Nature 352: 397-403

Sigmarsson O, Condomines M, Fourcade S (1992) A detailed Th, Sr and O isotope study of Hekla : differentiation processes in an Icelandic Volcano. Contrib Mineral Petrol 112: 20-34

Sigmarsson O, Condomines M, Ibarrola E (1992) ^{238}U-^{230}Th radioactive disequilibria in historic lavas from the Canary Islands and genetic implications. J Volcanol Geotherm Res 54: 145-156

Sigmarsson O, Carn S, Carracedo JC (1998) Systematics of U-series nuclides in primitive lavas from the 1730-36 eruption in Lanzarote, Canary Islands and the implications for the role of garnet pyroxenite during oceanic basalt formation. Earth Planet Sci Lett 162: 1337-151

Sims KWW, DePaolo DJ, Murrell MT, Baldridge WS, Goldstein SJ, Clague DA (1995) Mechanisms of magma generation beneath Hawaii and mid-ocean ridges: uranium/thorium and samarium/neodymium isotopic evidence Science 267: 508-512

Sims KWW, DePaolo DJ, Murrell MT, Baldridge WS, Goldstein S, Clague D, Jull M (1999) Porosity of the melting zone and variations in the solid mantle upwelling rate beneath Hawaii : inferences from ^{238}U-^{230}Th-^{226}Ra and ^{235}U-^{231}Pa disequilibria. Geochim Cosmochim Acta 63: 4119-4138

Sleep NH (1990) Hotspots and mantle plumes : some phenomenology. J Geophys Res 95: 6715-6736

Späth A., A.P.L. Roex and R.A. Duncan, The geochemistry of lavas from the Comores archipelago, Western Indian Ocean: petrogenesis and mantle source region characteristics, J. Petrol., 37, 961-991, 1996

Spiegelman M Elliott T (1993) Consequences of melt transport for uranium series disequilibrium in young lavas. Earth Planet Sci Lett 118: 1-20

Stracke A, Salters VJM Sims KWW (1999) Assessing the presence of garnet-pyroxenite in the mantle sources of basalts through combined hafnium-neodymium-thorium isotope systematics. Geochem Geophys Geosyst 1: 1999GC000013

Turner S, Hawkesworth C, Rodgers N, King P (1997) U-Th disequilibria and ocean island basalt generation in the Azores. Chem Geol 139: 145-164

Vigier N, Bourdon B, Joron J-L Allègre CJ (1999) U-Th-Ra disequilibria in Ardoukoba tholeiitic basalts (Asal rift): timescales of crystallization. Earth Planet Sci Lett 174: 81-98

Watson S. and McKenzie D. (1991) Melt generation by plumes: a study of Hawaiian volcanism. J Petrol 32: 501-537

Wendlandt RF, Eggler DH (1980) The origins of potassic magmas: 2. Stability of phlogopite in natural spinel lherzolite and in the system $KalSi\ O_4$-MgO-H_2O-CO_2 at high pressures and high temperatures. Am J Sci 280: 421-458

Widom E, Schmincke H-U, Gill J (1992) Processes and timescales in the evolution of a chemically zoned trachyte : Fogo A, Sao Miguel, Azores. Contrib Mineral Petrol 111: 311-328

Widom RE, Carlson RW, Gill JB, Schmincke H-U (1997) Th-Sr-Nd-Pb isotope and trace element evidence for the origin of the Saõ Miguel, Azores enriched mantle source. Chem Geol 140: 49-68

Williams RW, Gill JB (1989) Effects of partial melting on the uranium decay series, Geochim Cosmochim Acta 53: 1607-1619

Wilson TJ (1963) A possible origin of the Hawaian islands. Canad J Phys 41: 863-870

Zimmerman ME, Zhang S, Kohlstedt DL, Karato S (1999) Melt Distribution in Mantle Rocks Deformed in Shear. Geophys Res Lett 26:1505-1508

Zindler A, Hart SR (1986) Chemical Geodynamics. Ann Rev Earth Planet Sci 14:493-571

Zindler A, Staudigel H, Batiza R (1984) Isotope and trace element geochemistry of young Pacific seamounts: implications for the scale of upper mantle heterogeneity. Earth Planet Sci Lett: 70: 175-190

Table 1. Main parameters used in melting models

Parameters	*Notation*	*Units*	*Range*
Degree of melting	F	none	0-0.2
Upwelling rate	W	$m.a^{-1}$	0-1
Melting rate	Γ	$kg.m^{-3}.a^{-1}$	10^{-3}-10^{-5}
Solidus temperature	T	K	1000-1400
Length of melting column	Z	km	0-50
Plate velocity		$m.a^{-1}$	0.01-0.1
Matrix porosity	ϕ	none	0-0.05
Solid density	ρ_s	$kg.m^{-3}$	3350
Melt density	ρ_m	$kg.m^{-3}$	2700
Lithosphere thickness	h	km	0-100

Table 2 Experimentally determined mineral/melt partition coefficients for U, Th, and Ba in Cpx and Gt and bulk partition coefficients calculated for a garnet peridotite source

	Clinopyroxene			*Garnet*			*Garnet Peridotite*			
(x10^3)	*U*	*Th*	*Ba*	*U*	*Th*	*Ba*	*U*	*Th*	*Ra*	*Pa*
Beattie	0.9	1.3	0.5	9.6	1.5	0.01	1.2	0.29	0.04	
Salters & Longhi	3.5	3.5	**	41	1.5	**	5.3	2.6		**
La Tourrette et al.	4.5	10	**	15	19	**	2.2	1.0		**
Lundstrom et al.	10	15	**	**	1.7	**	2.6	1.4	(0.01)	(0.13)

Experimentally determined mineral/melt partition coefficients for U, Th, and Ba in Cpx and Gt from Beattie, 1993a, b; La Tourette et al., 1992; 1993; Lundstrom et al., 1994; Salters and Longhi, in review. Bulk partition coefficients for garnet peridotite source calculated using Ol = 59%, Opx = 21%, Cpx = 8%, Gt = 12%. Lundstrom et al. (1994) bulk D values use D^{U} and D^{Th} for garnet from La Tourrette et al. (1993) and assume that $D^{Pa}=D^{U5+}$ and D^{Ra} =1.0E-5. Beattie bulk D^{Ra} value assumes that $D^{Ra\ a}\ D^{B\ a}$. The inverted D^{U}-D^{Th} and D^{U} and D^{Pa} values are from correlations of (^{230}Th/^{238}U) and (^{231}Pa/^{235}U) with Sm/Nd fractionation (Figure 3) (see Sims et al. 1995 for details) and are in the range of bulk D values calculated from experimental measurements. This inversion is based upon the equations for batch melting and does not account for the contribution of ingrown ^{230}Th and ^{231}Pa in the measured (^{230}Th/^{238}U) and (^{231}Pa/^{235}U) disequilibria; therefore these estimates of the bulk D^{U}, D^{Th} and D^{Pa} maximize U/Th and U/Pa fractionation.

Figure 1

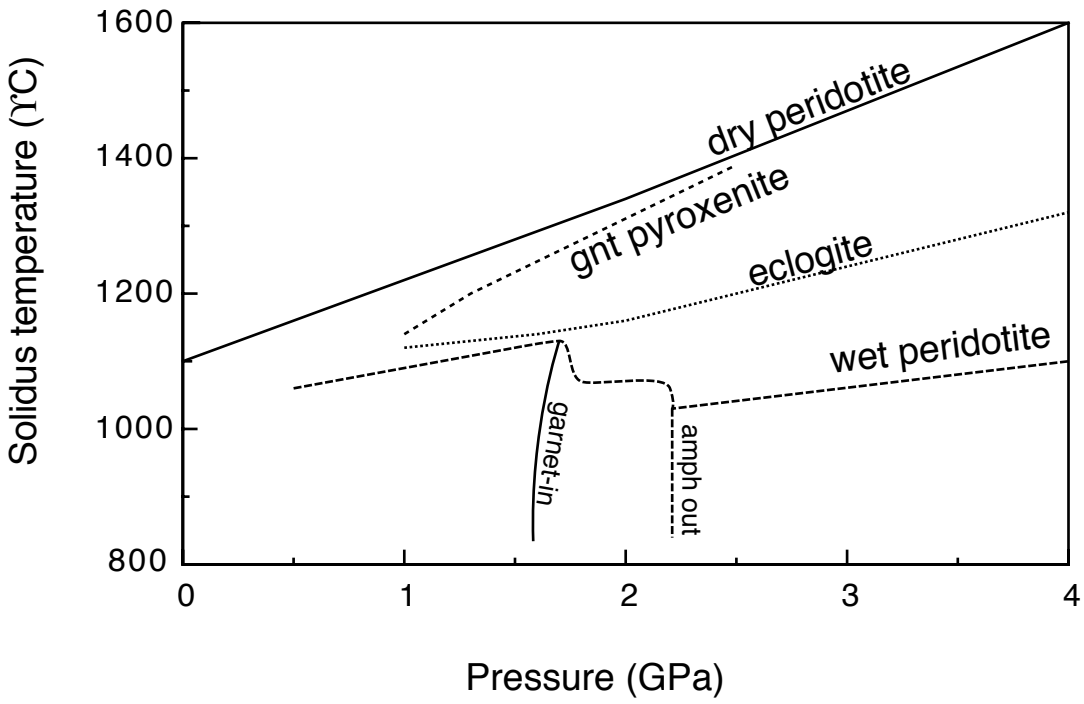
1600
1400
1200
1000
800
0
1
2
3
4
Solidus temperature (°C)
Pressure (GPa)
dry peridotite
gnt pyroxenite
eclogite
wet peridotite
garnet-in
amph out

Figure 2

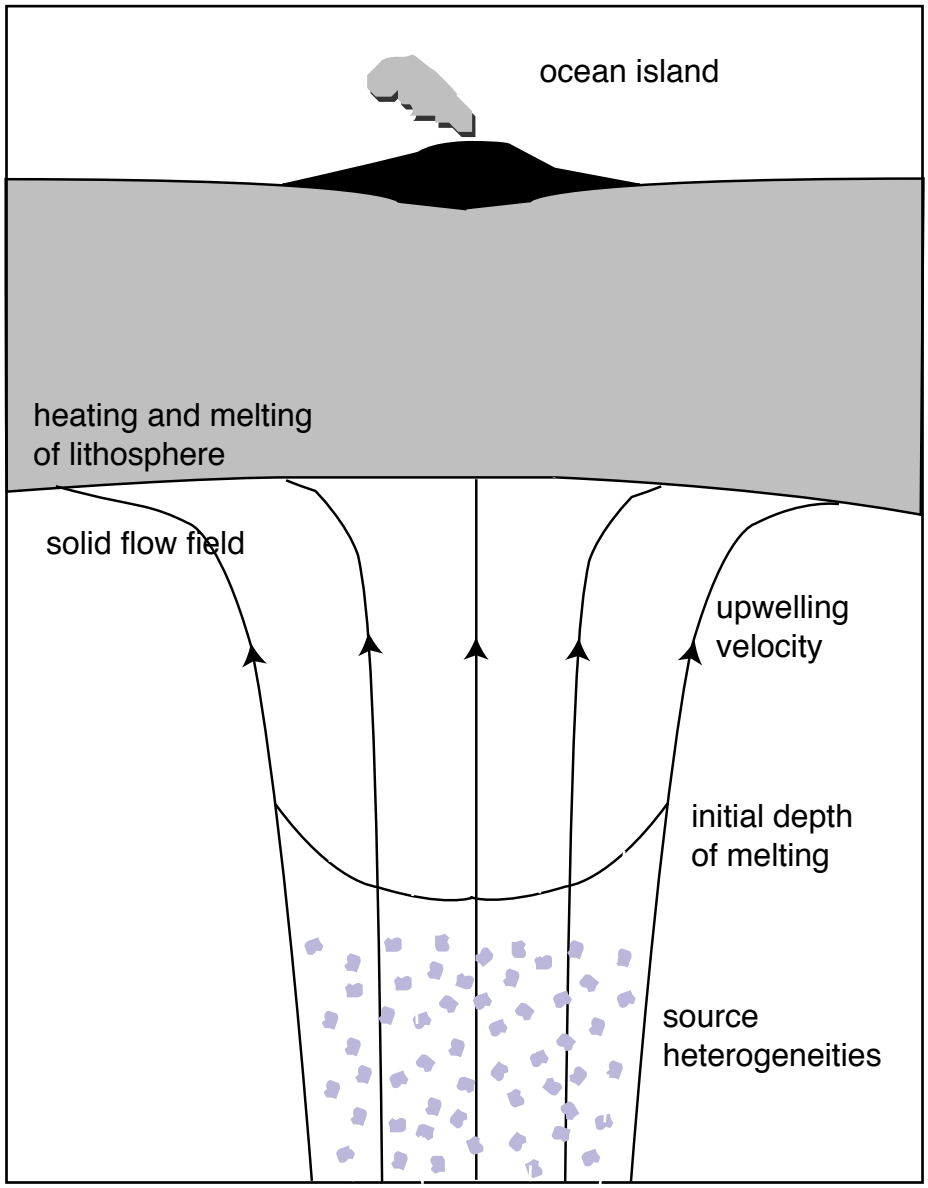
ocean island
heating and melting
of lithosphere
solid flow field
upwelling
velocity
initial depth
of melting
source
heterogeneities

Figure 3

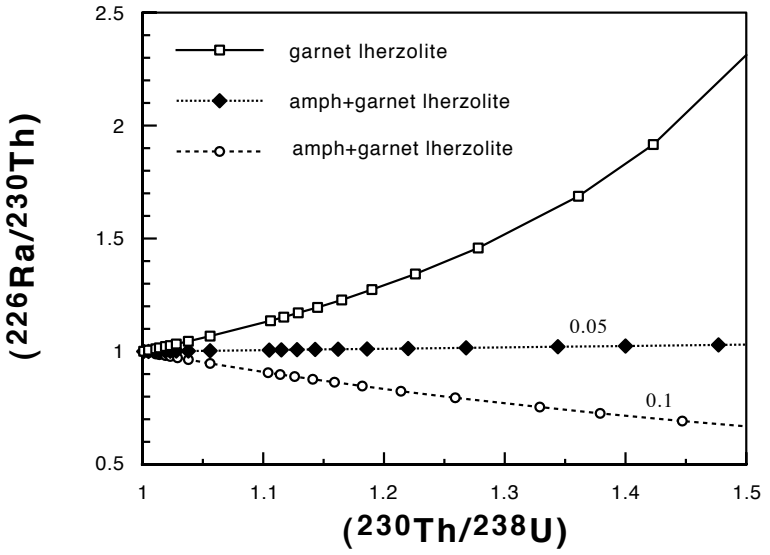
garnet lherzolite
amph+garnet lherzolite
amph+garnet lherzolite
0.05
0.1
(226Ra/230Th)
(230Th/238U)

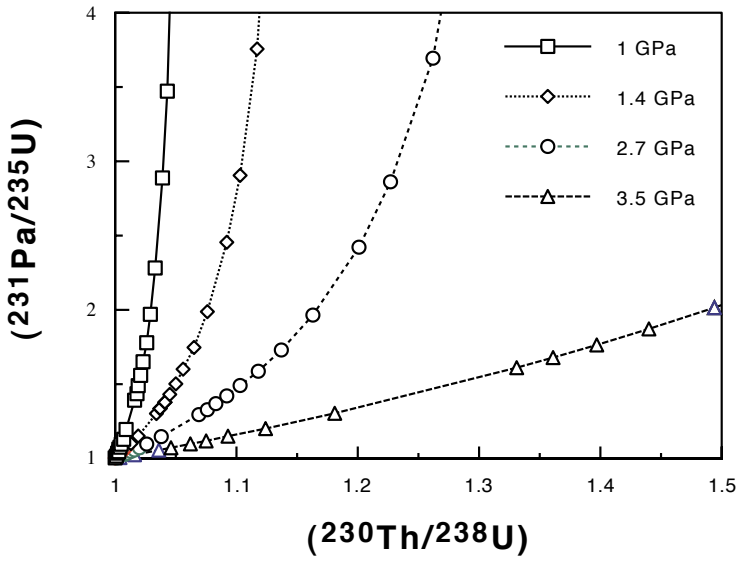
1 GPa
1.4 GPa
2.7 GPa
3.5 GPa
(231Pa/235U)
(230Th/238U)

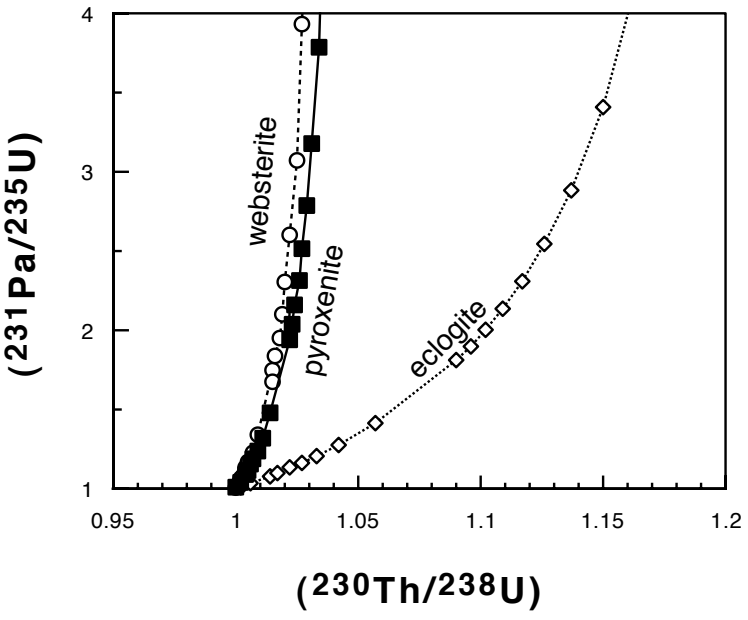
websterite
pyroxenite
eclogite
(231Pa/235U)
(230Th/238U)

Figure 4

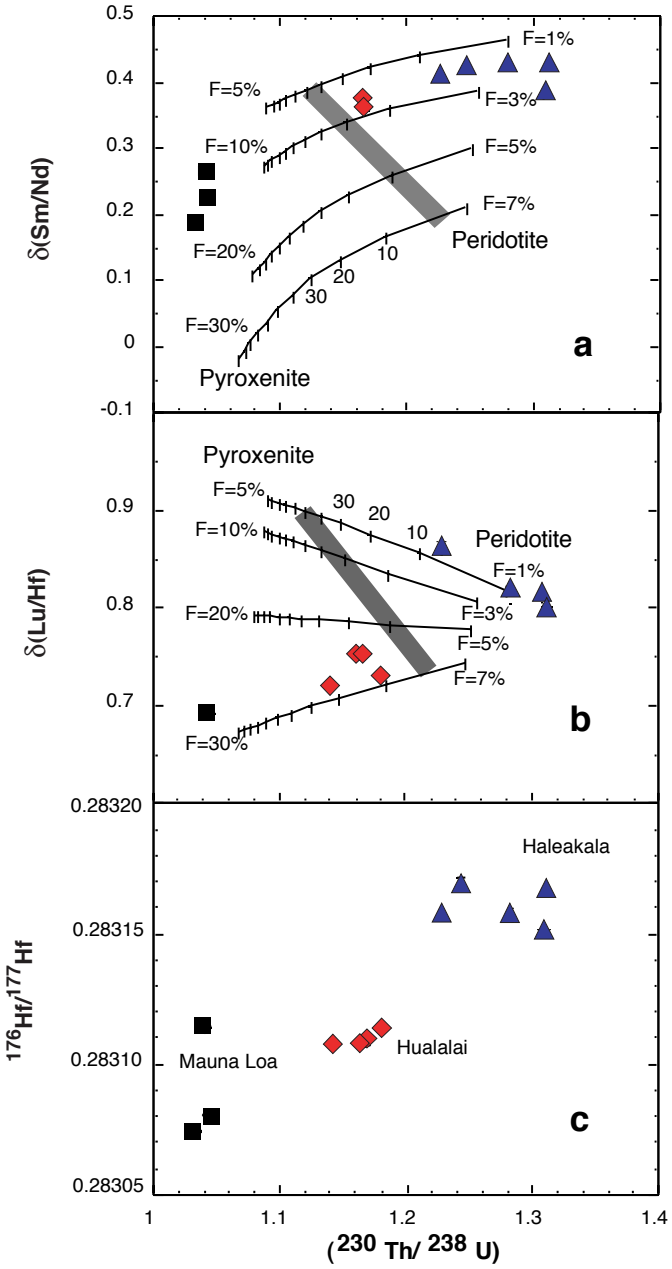
δ(Sm/Nd)
F=1%
F=5%
F=3%
F=10%
F=5%
F=7%
Peridotite
F=20%
10
20
30
F=30%
Pyroxenite
a
δ(Lu/Hf)
Pyroxenite
F=5%
30
20
F=10%
10
Peridotite
F=1%
F=20%
F=3%
F=5%
F=7%
F=30%
b
176Hf/177Hf
Haleakala
Mauna Loa
Hualalai
c
(230 Th/ 238 U)

Figure 5

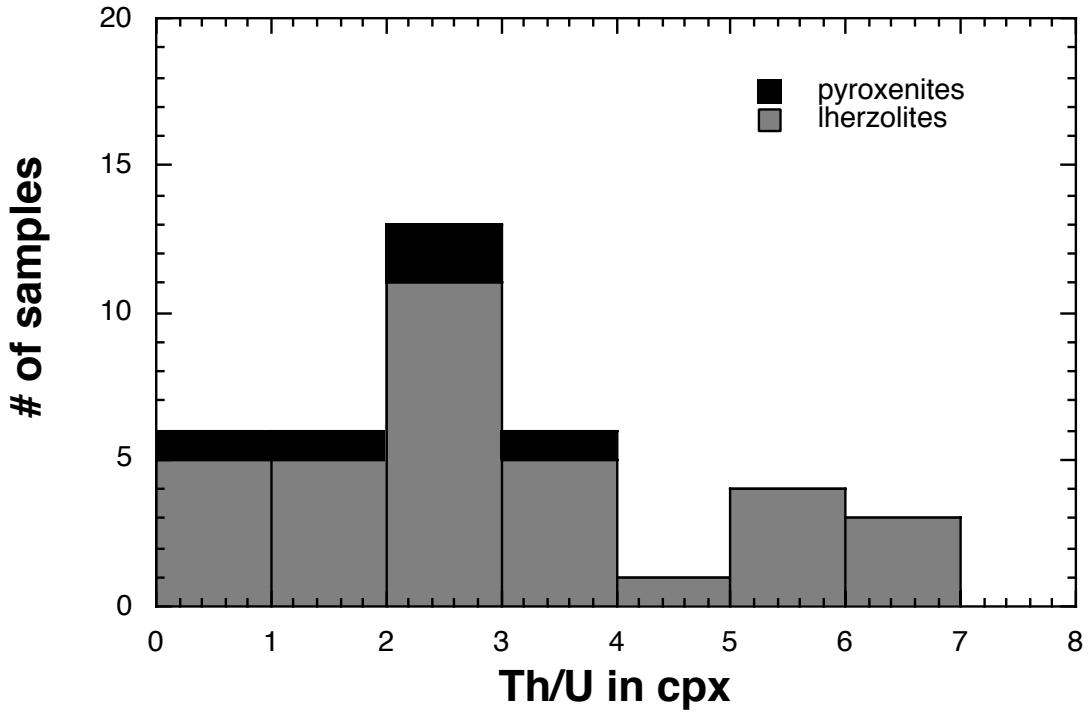
20
15
10
5
0
# of samples
0
1
2
3
4
5
6
7
8
Th/U in cpx
pyroxenites
lherzolites

Figure 6

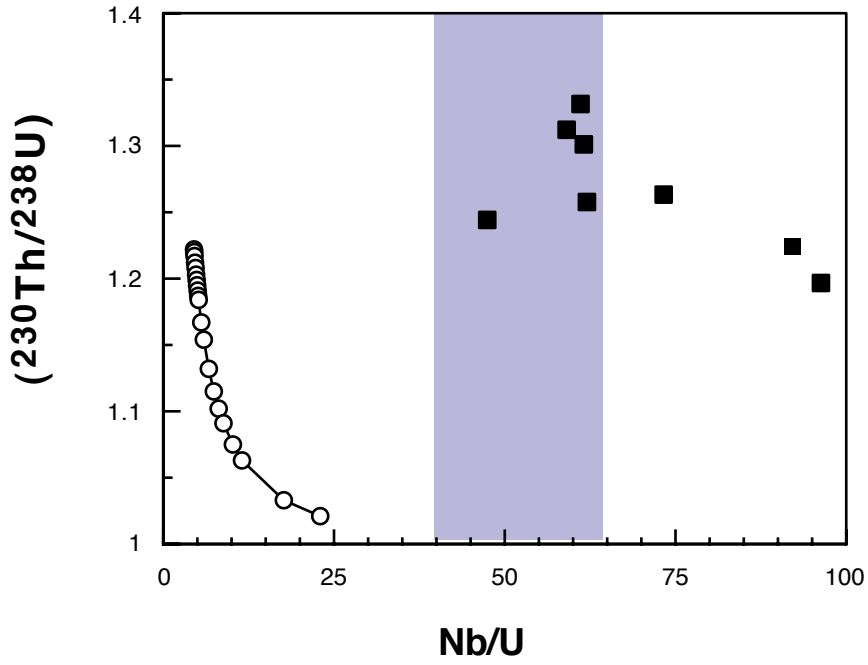

Figure 7

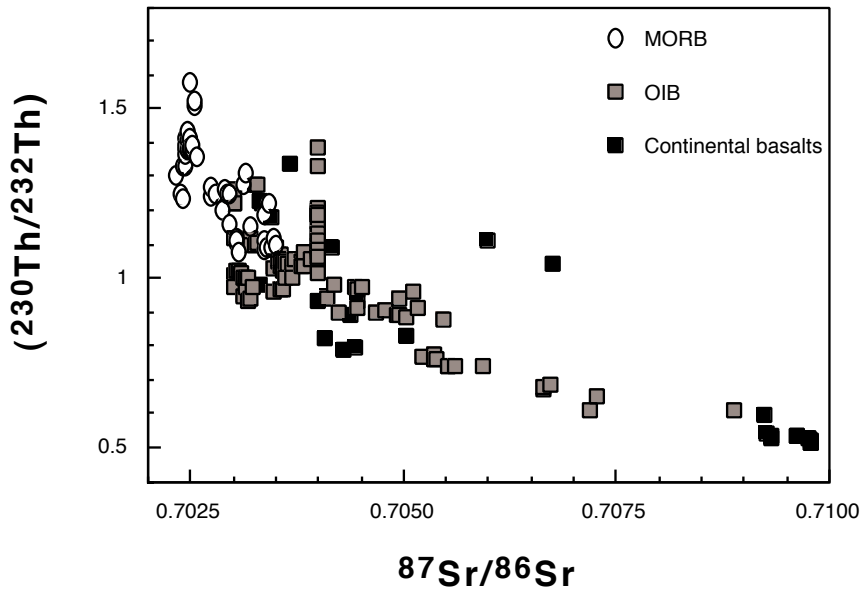
MORB
OIB
Continental basalts
1.5
1
0.5
0.7025
0.7050
0.7075
0.7100
(230Th/232Th)
87Sr/86Sr

Figure 8

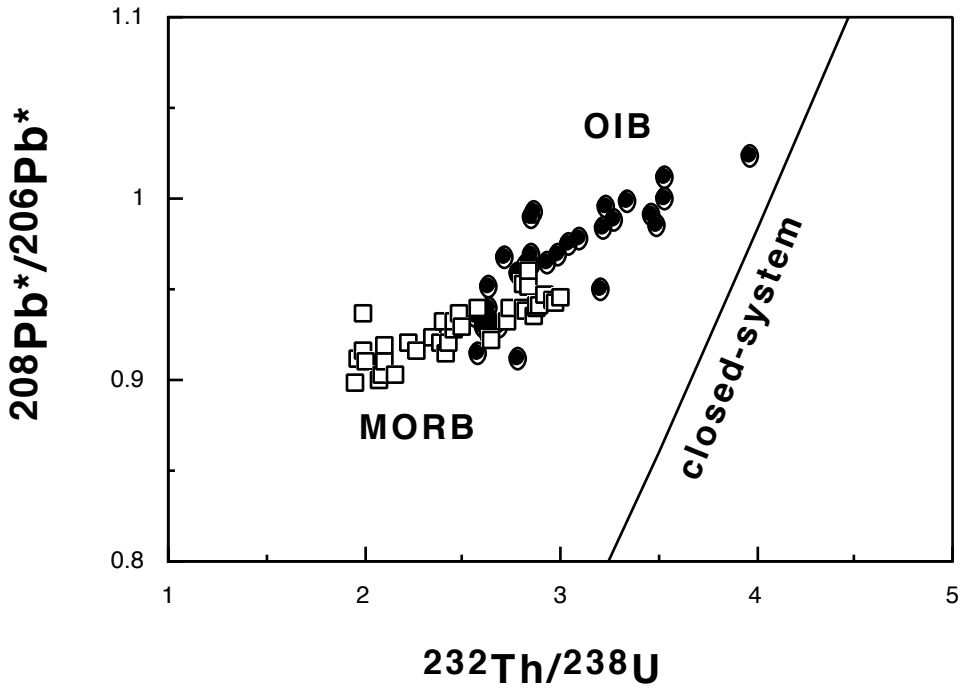
1.1
1
0.9
0.8
1
2
3
4
5
OIB
MORB
closed-system
208Pb*/206Pb*
232Th/238U

Figure 9 A

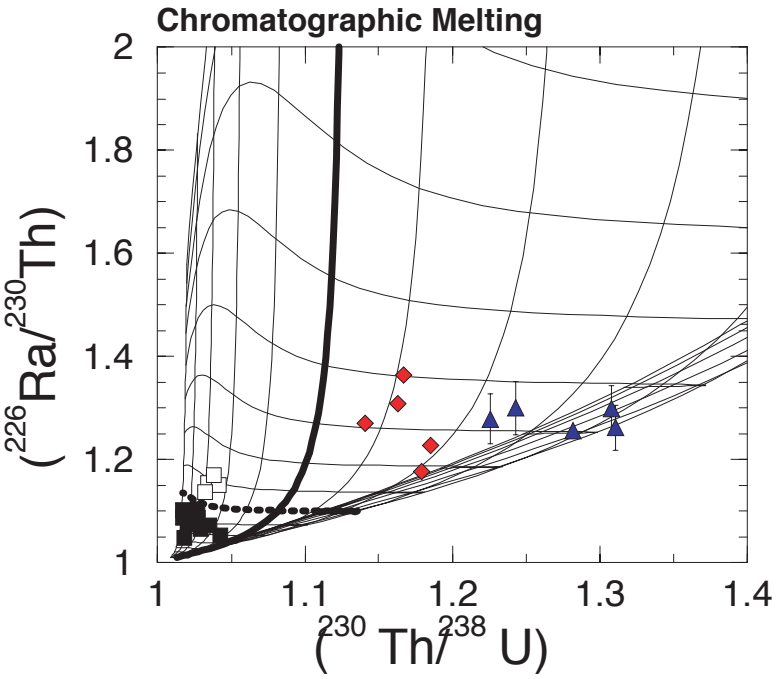

Figure 9 B

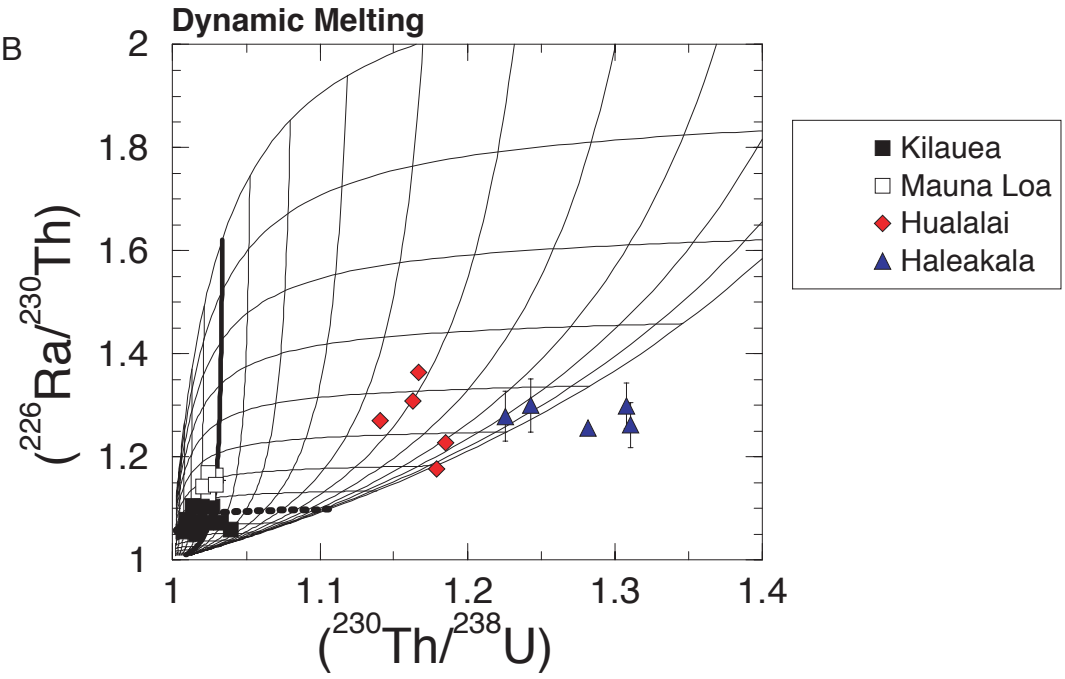

Figure 10 A

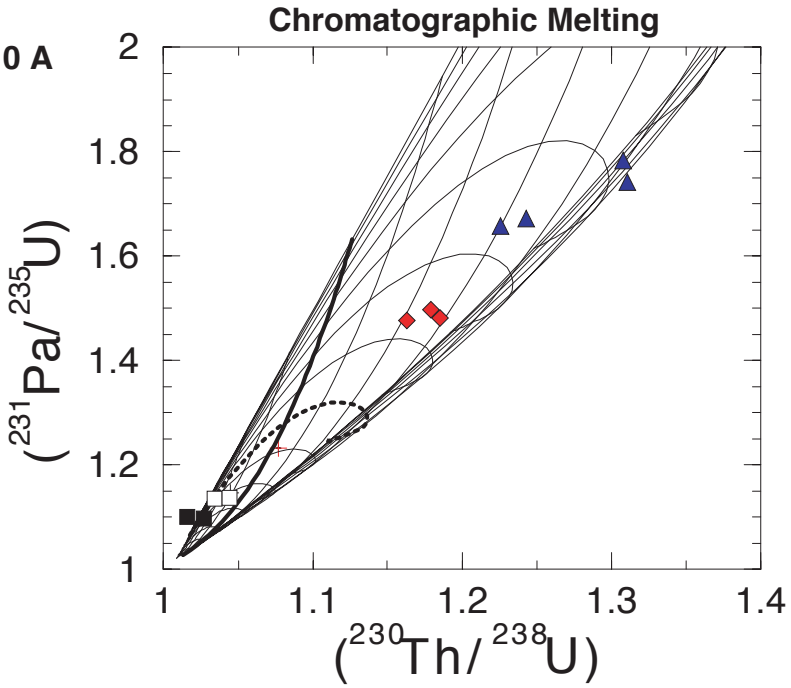

Figure 10 B

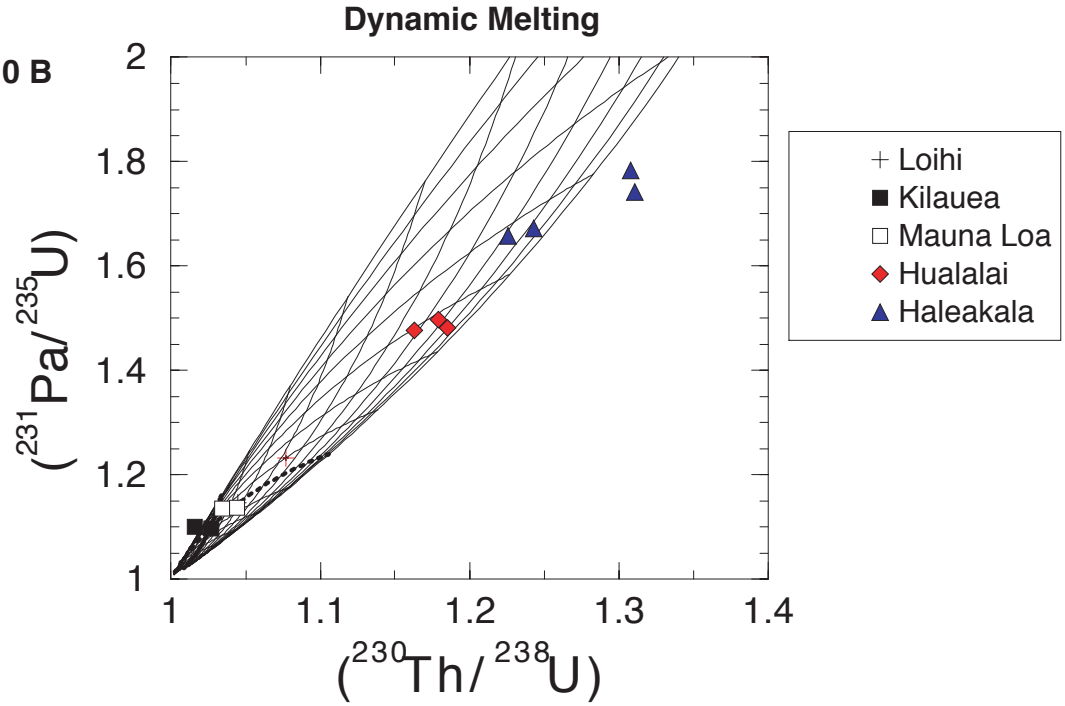

Figure 11

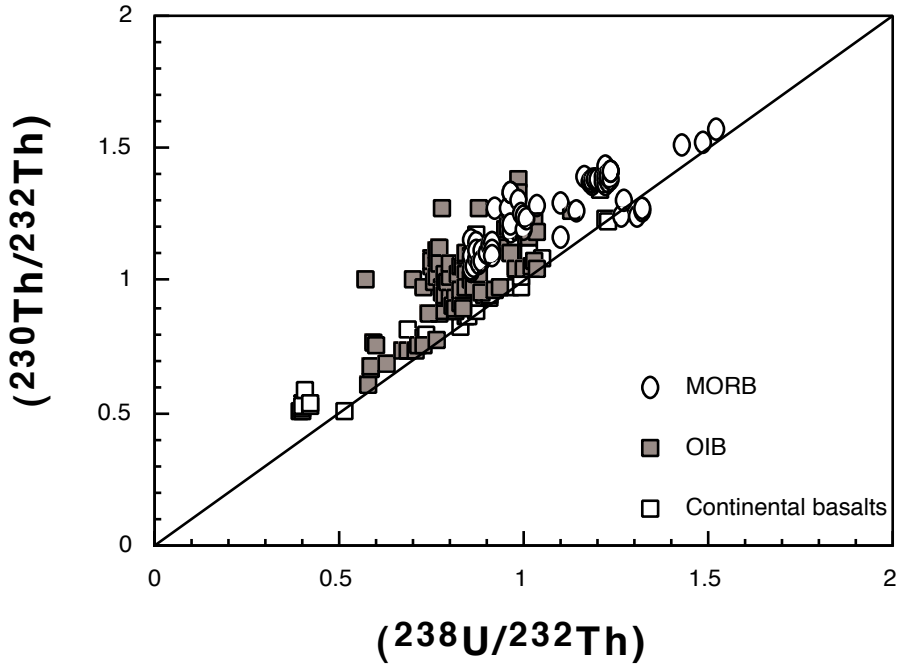
2
1.5
1
0.5
0
0
0.5
1
1.5
2
(230Th/232Th)
(238U/232Th)
MORB
OIB
Continental basalts

Figure 12

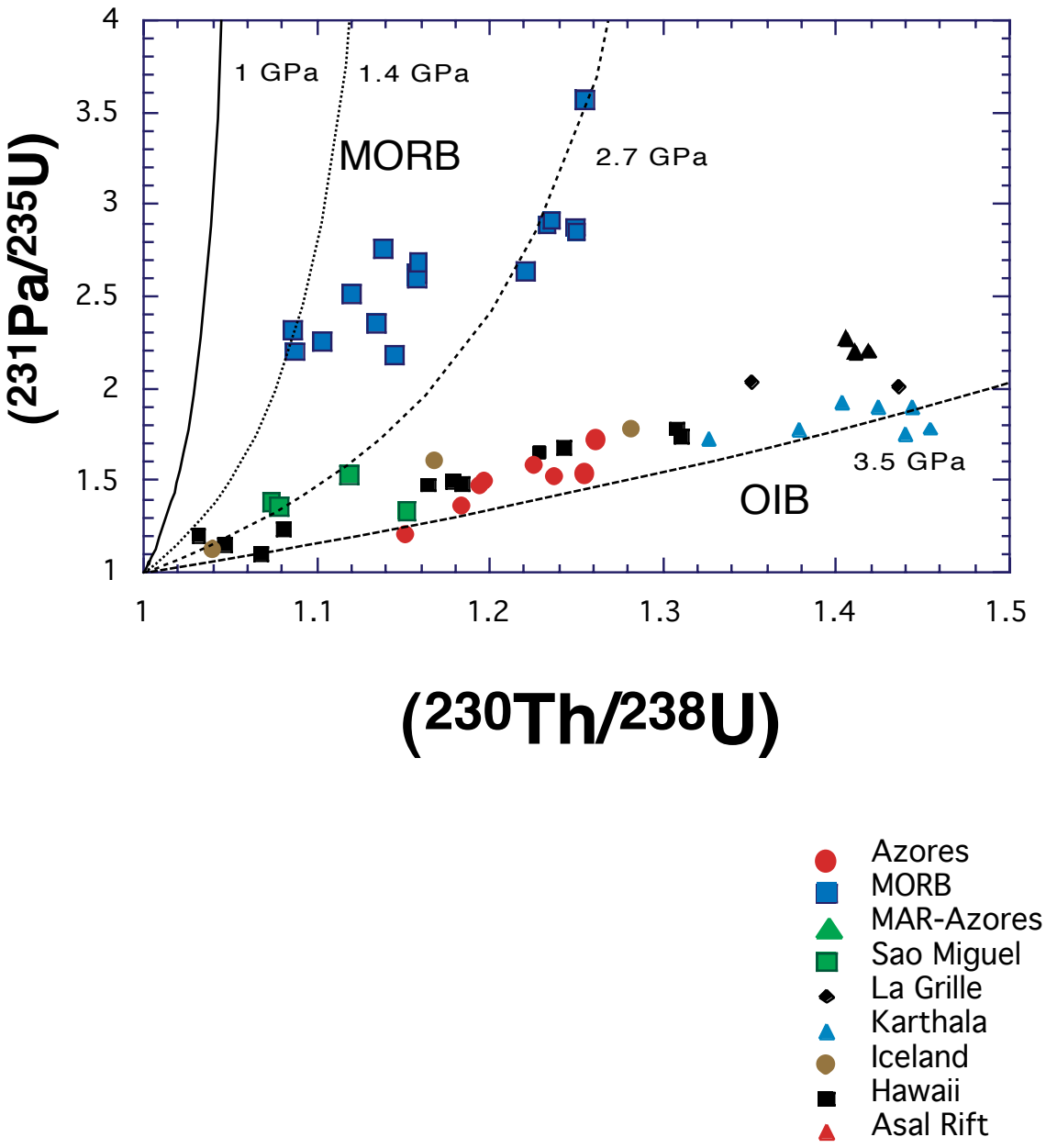
4
3.5
3
2.5
2
1.5
1
1
1.1
1.2
1.3
1.4
1.5
1 GPa
1.4 GPa
2.7 GPa
3.5 GPa
MORB
OIB
(231Pa/235U)
(230Th/238U)
Azores
MORB
MAR-Azores
Sao Miguel
La Grille
Karthala
Iceland
Hawaii
Asal Rift

Figure 13

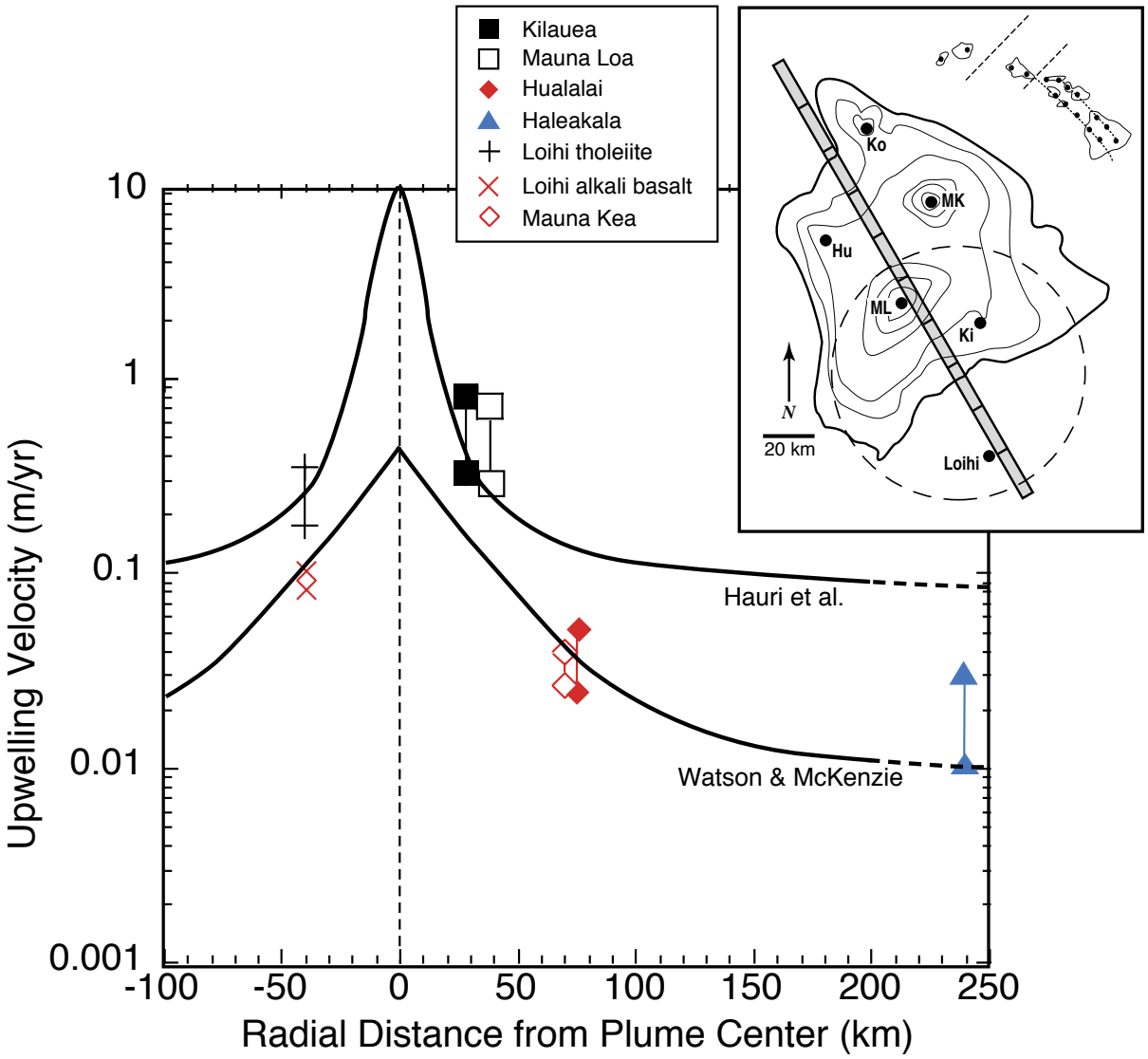
Kilauea
Mauna Loa
Hualalai
Haleakala
Loihi tholeiite
Loihi alkali basalt
Mauna Kea
Ko
MK
Hu
ML
Ki
Loihi
N
20 km
Hauri et al.
Watson & McKenzie
Upwelling Velocity (m/yr)
10
1
0.1
0.01
0.001
-100
-50
0
50
100
150
200
250
Radial Distance from Plume Center (km)

Figure A1

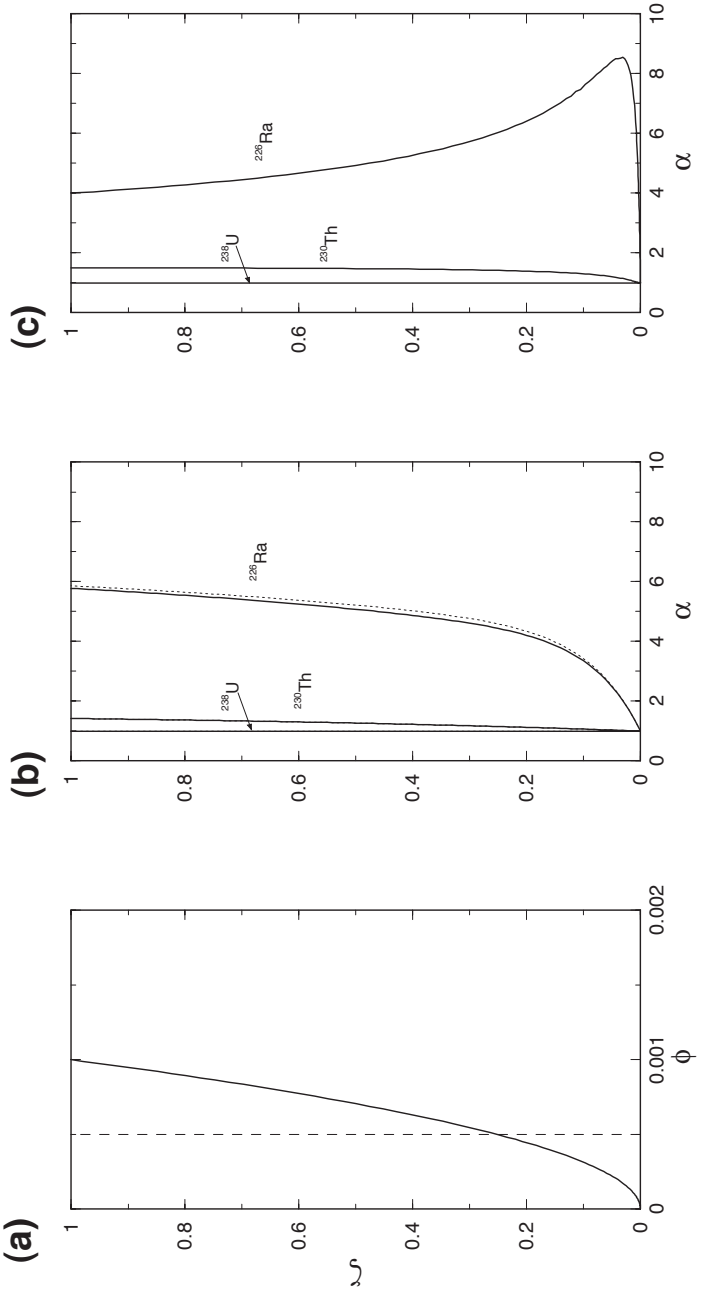

Figure A2

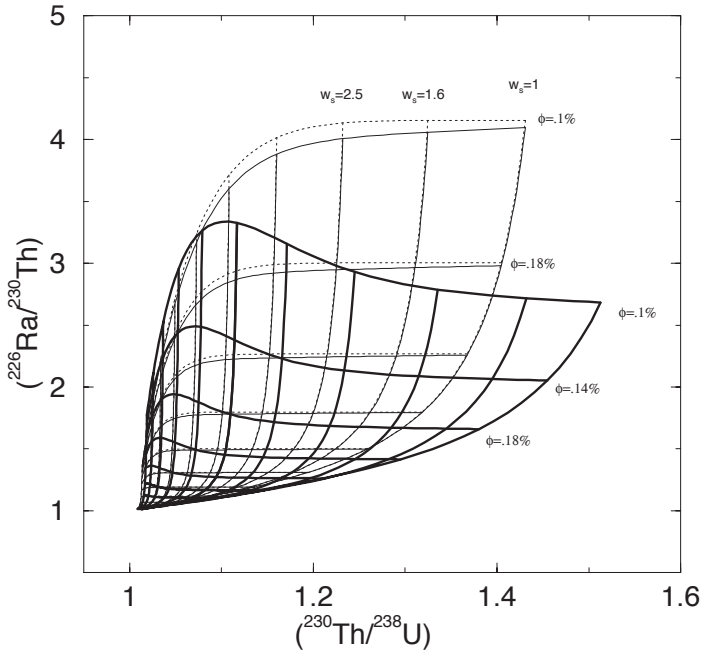
5
4
3
2
1
1
1.2
1.4
1.6
(^{226}Ra/^{230}Th)
(^{230}Th/^{238}U)
w_s=2.5
w_s=1.6
w_s=1
ϕ=.1%
ϕ=.18%
ϕ=.1%
ϕ=.14%
ϕ=.18%